Transcriptomic profiling of macrophage polarization

Serena X. Liu

A dissertation

submitted in partial fulfillment of the

requirements for the degree of

Doctor of Philosophy

University of Washington

2020

Reading Committee:

Cole Trapnell, Chair

David Hawkins

Suzie Pun

Program Authorized to Offer Degree:

Genome Sciences

University of Washington

Abstract

Transcriptomic profiling of macrophage polarization

Serena X. Liu

Chair of the Supervisory Committee:
Associate Professor Cole Trapnell
Genome Sciences

Macrophages perform a wide variety of crucial, and sometimes contradictory, functions. While “pro-inflammatory” activities like fighting off infections and “anti-inflammatory” activities like wound-healing traditionally have been attributed to M1 and M2 macrophage subsets, studies of macrophages in both *in vitro* and *in vivo* contexts suggest that macrophages are phenotypically plastic and may shift states in response to environmental changes. However, it remains unclear whether macrophages retain any persistent memory of past polarization states which may then impact their future repolarization to new states.

In this dissertation, I first describe the evolving understanding of macrophage polarization and phenotypic plasticity and introduce commonly used models for macrophage polarization in humans and mice. I also outline recent advances in single-cell RNA-sequencing

and some of the most popularly used platforms for single-cell transcriptomics. I then focus on my work characterizing macrophage polarization and repolarization *in vitro*, where I performed deep transcriptomic profiling at high temporal resolution as macrophages were polarized with cytokines that drive them into “M1” and “M2” molecular states. I find through trajectory analysis of their global transcriptomic profiles that macrophages which are first polarized to M1 or M2 and then subsequently repolarized demonstrate little to no memory of their polarization history. I observe complete repolarization both from M1 to M2 and vice versa, and I find that macrophage transcriptional phenotypes are defined by the current cell microenvironment, rather than an amalgamation of past and present states. In the following chapters, I present preliminary work aimed at characterizing alveolar macrophages, the tissue-resident macrophages of the lung: I first describe my attempts to identify key stimuli for triggering specification of alveolar macrophage fate. I then discuss preliminary results from single-cell RNA-seq profiling of alveolar macrophages in the context of pulmonary alveolar proteinosis. In the final chapter, I reflect on challenges I faced in adapting single-cell RNA-sequencing methods to work with primary tissue cells and summarize the main findings from my work.

TABLE OF CONTENTS

LIST OF FIGURES

LIST OF TABLES

ACKNOWLEDGEMENTS

As a graduate student, I have been incredibly lucky to be part of a diverse and welcoming community at the University of Washington. Thank you to the members of UW Genome Sciences and the eScience community for creating a supportive and inspiring environment to do science and pursue a love of learning.

I thank my advisor Cole Trapnell for his infectious optimism and unrelenting support through all the bumps in the road. I admire many things about Cole: his dedication to fostering an inclusive and engaging lab environment and to ensuring the wellbeing of his lab members; his incredible knack for breaking down even the most technical topics in a way that is easily accessible; his commitment to rigorous and meaningful science. I always leave conversations with you newly inspired.

I thank my committee members, David Hawkins, Suzie Pun, Daniela Witten, and April Stempien-Otero for generously offering your guidance and expertise. Without your well-timed advice, I may not have considered studying macrophage depolarization in addition to repolarization, and would have missed half the story! I am also grateful to David Beck, Magdalena Balazinska, and other members of the eScience Institute for teaching me the ins and outs of data science, and for creating such a welcoming community to connect with graduate students and post-docs across different departments and share our unique “big data” problems.

I thank my past scientific mentors, particularly Thomas Jack. You were the one who first stoked my enthusiasm in pursuing scientific research as a career; thank you for your tireless

patience in office hours and in lab, and for humoring and nurturing the curiosity of a college freshman new to genetics.

I thank the past and present members of the Trapnell lab, especially Jose Luis McFaline-Figueroa, Dana Jackson, Sanjay Srivatsan, David Read, and Jonathan Packer for many late night (and late morning) conversations, and for generously sharing your time and expertise. You have saved me much frustration (and much wasted time due to inefficient code, thank you Jonathan!), and it has been a pleasure and an honor to be your colleague.

I thank my collaborator Heather Gustafson, who taught me everything I know about macrophages and who dedicated countless hours to helping me establish my protocols and culture systems for bone marrow-derived macrophages. I am also grateful to Scott Furlan, for being an invaluable sounding board on immune cell related matters. Thanks also to Bruce Trapnell, Paritha Arumugam, Brenna Carey, and our other collaborators from Cincinnati Children's Hospital for your dedication and support, and for your patience and help in wrangling regular sample shipments halfway across the country.

I am immensely grateful to my friends for keeping me sane throughout this journey. Thank you to Katherine Xue and Seungsoo Kim for dragging me out to Century Ballroom and getting me back into West Coast Swing; to Clara Amarosi, Emily Killingbeck, and Claudia Espinoza for the lunch get-togethers and the study sessions that eventually morphed into writing sessions; to Aditi Misra, Lauren Heywood, Chloe Lee, Kristy Choi, and Rachel Aragon for your unflagging support and lighthearted distractions – thank you for supplying the cute dog photos I need in my life.

Finally, I thank my family for their encouragement and unconditional support; without you, none of this would be possible.

Chapter 1. INTRODUCTION

1.1 MACROPHAGES: THE M1/M2 PARADIGM AND THE KEY ROLE OF PHENOTYPIC PLASTICITY

Macrophages were first discovered in the late 19th century by Elie Metchnikoff, who identified them as phagocytic cells that facilitated pathogen elimination. Metchnikoff found that macrophages from previously infected animals were more effective at killing bacteria and thus proposed the concept of macrophage activation, whereby macrophages that have been exposed to pathogens enter an activated state and become more efficient bacterial killers (Liu et al., 2014). Subsequent research revealed that cellular factors could promote resistance to infection even without any pathogenic exposure, and in the early 1980's, interferon-γ (IFN-γ) was identified as a cytokine that could independently induce macrophage activation (Nathan et al., 1983). Macrophages stimulated with IFN-γ displayed stronger antigen presenting capacity, increased phagocytosis, and secretion of more pro-inflammatory cytokines and toxic mediators, and became known as "classically activated" or M1 macrophages. *In vivo*, M1 macrophages were typically generated as products of a cell-mediated immune response, and displayed strong microbicidal and tumoricidal activity (Mosser and Edwards, 2008; Sica and Mantovani, 2012). A decade later, interleukin (IL)-4 and IL-13 were discovered to induce a different activated macrophage state, in which major histocompatibility class (MHC) II antigen expression was upregulated but inflammatory cytokine production was inhibited; these IL-4/IL-13-activated macrophages were dubbed "alternatively activated" or M2 macrophages (Gordon, 2003; Stein et al., 1992). M2

macrophages secrete components of the extracellular matrix and are thought to play a key role in wound healing and tissue repair (Mosser and Edwards, 2008).

M1 and M2 macrophages were initially viewed as distinct macrophage subtypes with unique and opposing activities: M1 macrophages were pro-inflammatory, immunogenic, and tissue destructive, while M2 macrophages were anti-inflammatory, tissue restorative, and promoted immune tolerance (Goerdt et al., 1999; Gordon, 2003; Mills et al., 2000; Stout and Suttles, 1997). As additional intermediate macrophage states were discovered (Mantovani et al., 2004; Wong et al., 2010; Xue et al., 2014), a spectrum model for macrophage activation emerged, wherein M1 and M2 macrophages represented the extreme ends of a continuum of functional states (Biswas and Mantovani, 2010; Mantovani et al., 2002; Martinez and Gordon, 2014; Mosser and Edwards, 2008). However, it remains unclear whether macrophages occupy a truly continuous spectrum, or whether discrete intermediate phenotypes exist along the spectrum between M1 and M2. Moreover, some researchers have suggested that the documented intermediate macrophage phenotypes may simply represent varying mixtures of M1- and M2-type macrophages (Mills and Ley, 2014).

Studies of macrophage activation have revealed that macrophages remain phenotypically plastic and can shift their functional phenotype in response to signals in their local microenvironment, both *in vitro* (Gosselin et al., 2014; Hagemann et al., 2006; Stout and Suttles, 2004; Stout et al., 2005) and *in vivo* (Guiducci et al., 2005; Lavin et al., 2014). This phenotypic plasticity challenges the view of M1 and M2 macrophages as irreversibly differentiated cell subtypes and suggests that M1 and M2, as well as other intermediate macrophage phenotypes, might instead represent transient functional states dependent on the macrophage environment.

Outside the context of M1/M2 phenotypes, macrophage plasticity is also thought to play an important role in mediating the function of tissue-resident macrophages.

1.2 TISSUE-RESIDENT MACROPHAGES

Tissue-resident macrophages are present in almost all tissues in the body, forming local, self-maintaining populations separate from blood monocyte-derived macrophages, and they exhibit highly heterogeneous phenotypes as a consequence of functional adaptation to different tissue environments (Davies et al., 2013; Murray and Wynn, 2011; Wynn et al., 2013). Tissue-resident macrophages play a crucial role in maintaining tissue homeostasis, and they perform a wide array of niche-specific functions: surfactant clearance in the lung (Nakamura et al., 2013; Trapnell and Whitsett, 2002), neural pruning in the brain (Nayak et al., 2014; Paolicelli et al., 2011), maintaining immunological tolerance and mediating metabolic adaptation in the liver (Ju and Tacke, 2016; Olefsky and Glass, 2010; Sica et al., 2014; Zimmermann et al., 2012), erythrocyte clearance and iron metabolism in the spleen (Kohyama et al., 2009), and facilitating adaptive thermogenesis in adipose tissue (Nguyen et al., 2011), among others. In addition to carrying out these tissue-specific activities, macrophages must also fulfill systemic duties such as immune surveillance and mediating host responses to infection and injury (Davies et al., 2013; Murray and Wynn, 2011). Phenotypic plasticity may contribute to macrophages' ability to carry out a wide range of diverse functions and to counterbalance local and systemic roles; however, while some of the individual factors modulating macrophage plasticity have been identified (Okabe and Medzhitov, 2014), the molecular mechanisms underlying this plasticity remain largely unknown.

1.3 MACROPHAGES IN DISEASE

Macrophage malfunction has been implicated in a wide array of diseases, including asthma (Kim et al., 2010; Melgert et al., 2010, 2011), pulmonary alveolar proteinosis (PAP) (Nakamura et al., 2013; Trapnell and Whitsett, 2002; Trapnell et al., 2003), obesity (Kanda et al., 2006; Lumeng et al., 2007; Weisberg et al., 2003; Xu et al., 2003), cancer (Mantovani et al., 2011; Murray and Wynn, 2011; Qian and Pollard, 2010; Sica and Mantovani, 2012; Wynn et al., 2013), and atherosclerosis (Hansson and Hermansson, 2011; Libby et al., 2011; Murray and Wynn, 2011). In many of these cases, macrophages are thought to play a key role in disease pathogenesis and are considered a promising therapeutic target. For example, pulmonary alveolar proteinosis is caused by a deficiency in GM-CSF signaling in alveolar macrophages, and can be successfully treated by transplanting macrophages with normal GM-CSF signaling into the lungs of affected patients (Suzuki et al., 2014; Trapnell et al., 2003).

Macrophages have also been shown to play a critical role in cancer: macrophages often form a large part of tumor bodies, and these tumor-associated macrophages (TAMs) have been reported to promote tumor initiation, progression, and metastasis (Qian and Pollard, 2010; Wynn et al., 2013). Tumor-promoting TAMs typically exhibit an immunosuppressive “M2-like” phenotype, while antitumor TAMs display a more “M1-like” phenotype (Andreu et al., 2010; DeNardo et al., 2009, 2010; Mantovani et al., 2002; Qian and Pollard, 2010). Efforts to combat tumor progression by repolarizing TAMs from an M2-like phenotype towards an M1-like phenotype have shown some success (Duluc et al., 2009; Goubau et al., 2009; Guiducci et al., 2005; Hagemann et al., 2008; Watkins et al., 2009). Alternatively, other macrophage-based cancer therapies aim to limit tumor growth by reducing TAM recruitment or function (Abraham et al., 2010; Aharinejad et al., 2009).

In the case of obesity, accumulation of adipose tissue macrophages (ATMs) plays a key role in disease progression, and the number of ATMs present strongly correlates with bodyweight, body mass index, and total body fat (Subramanian and Ferrante, 2009). Macrophage polarization also appears to be closely tied to disease pathogenesis: ATMs in obese individuals are polarized towards an M1-like phenotype, while ATMs in lean individuals are polarized towards an M2-like phenotype (Sica and Mantovani, 2012). Moreover, diet-induced weight gain in mice is associated with an ATM phenotypic shift from M2-like to M1-like, and weight loss is associated with a converse shift from M1-like to M2-like (Kosteli et al., 2010; Lumeng et al., 2007). Consequently, developing a better understanding of the molecular mechanisms controlling phenotypic shifts between M1- and M2-like states may give insight into the etiology of obesity and may lead to the discovery of novel therapeutic targets.

1.4 MODELS OF MACROPHAGE POLARIZATION IN MICE AND HUMANS

To date, the two most commonly used *in vitro* macrophage model systems are 1) murine bone marrow-derived macrophages, and 2) human peripheral blood monocyte-derived macrophages (Murray et al., 2014). A combination of IFN-γ and lipopolysaccharide (LPS) or tumor necrosis factor-α (TNFα) are typically used to stimulate M1 activation, and IL-4 is used to stimulate M2 activation (Murray et al., 2014; Thomas and Mattila, 2014). These *in vitro* systems provide a cheap, simple, and reproducible means of studying macrophage activity and polarization. However, even within these relatively well-defined *in vitro* macrophage systems, macrophage behavior can vary based on factors such as the type of plastic used for cell culture, the types and sources of culture media and sera, and the length of cell exposure to cytokines (Thomas and Mattila, 2014). Additionally, macrophages cultured *in vitro* may not be fully representative of the

tissue-resident macrophages found *in vivo*, particularly since the bone marrow and circulating monocyte progenitors used in *in vitro* macrophage culture derive from hematopoietic stem cells, while tissue-resident macrophages arise from stem cells in the yolk sac and fetal liver (Epelman et al., 2014a). While circulating blood monocyte-derived macrophages are recruited to tissue reservoirs upon infection or injury, and these macrophages may more closely resemble the *in vitro* models, most populations of tissue-resident macrophages can maintain themselves via local proliferation under homeostatic conditions, and the degree of monocyte infiltration in homeostasis remains unknown (Epelman et al., 2014b; Hashimoto et al., 2013; Yona et al., 2013). Hence, some caution must be used when translating *in vitro* findings to *in vivo* conditions.

Mice are the predominant model for immunological research, particularly for *in vivo* work, and they closely mirror human biology in many respects (Mestas and Hughes, 2004). However, mice do differ from humans on some aspects of innate and adaptive immunity relevant to macrophage function. One primary difference concerns macrophage arginine metabolism. In mice, M1 and M2 phenotypes can be clearly separated on the basis of arginine metabolism: IFN-γ and LPS induce expression of nitric oxide synthase (NOS) enzymes that convert arginine to nitric oxide (NO) in M1 macrophages, while IL-4 induces expression of arginase, which converts arginine into ornithine in M2 macrophages (Thomas and Mattila, 2014; Yeramian et al., 2006). Consequently, inducible nitric oxide synthase (iNOS) and arginase (or the corresponding metabolic products NO and ornithine) can be used as markers of M1 and M2 activation status in murine macrophages, and the existence of these clear-cut M1/M2 markers is one advantage of the mouse model system. In contrast, iNOS expression in human macrophages is much more controversial; while some researchers do not detect any NO production after stimulation with IFN-γ and LPS, other groups have observed NOS or arginase activity in human macrophages after such stimulation (Mestas and

Hughes, 2004; Schneemann and Schoeden, 2007; Schneemann and Schoedon, 2002; Thomas and Mattila, 2014). Due to these inconsistencies, iNOS and arginase cannot be used as definitive M1 and M2 markers in human macrophages, unlike in mice.

1.5 SINGLE-CELL RNA-SEQUENCING

In recent years, single-cell RNA-sequencing has developed into a robust and powerful tool for high-throughput, high-resolution transcriptomic analysis of cell states and dynamics. Single-cell approaches circumvent the averaging artifacts associated with traditional bulk population data, yielding new insights into the cellular diversity underlying superficially homogeneous populations. Single-cell RNA-seq technologies can quantify intra-population heterogeneity and allow study of cell states and transitions at very high resolution, potentially revealing cell subtypes or gene expression dynamics that are masked in bulk, population-averaged measurements (Trapnell et al., 2014; Wills et al., 2013). Thus far, single-cell RNA-seq has already shown great effectiveness both in unraveling complex cell populations (Cao et al., 2017; Grün et al., 2015; Jaitin et al., 2014; Shalek et al., 2013; Treutlein et al., 2014), enabling unsupervised learning of population structure and the discovery of novel subtypes and rare cell species, and in reconstructing developmental trajectories through dynamic processes like cell differentiation (Bendall et al., 2014; Cao et al., 2019; Tang et al., 2010; Trapnell et al., 2014).

The 10X Chromium platform for single-cell RNA-seq uses droplet-based microfluidic technology (Klein et al., 2015) to collect single-cell data. Briefly, single cells are captured in individual nanoliter emulsion droplets that each contain a labeled gel bead; these gel beads carry primers tagged with both a bead-specific barcode (the cell identifier) and a primer-specific barcode (a unique molecular identifier for each mRNA transcript captured). Within the droplets, cells are

lysed and their mRNA is captured by the gel bead primers, then reverse transcribed into cDNA; this cDNA, now labeled with cell-specific and transcript-specific barcodes, is subsequently amplified and used to prepare libraries for sequencing and downstream analysis. In this manner, the 10X platform is able to measure single-cell expression data for thousands of cells at a time.

An alternative approach uses **s**ingle-cell **c**ombinatorial **i**ndexing RNA-sequencing (sci-RNAseq) to collect transcriptomic data at single-cell resolution (Cao et al., 2017, 2019; Rosenberg et al., 2018). sci-RNAseq relies on a "split-and-pool" approach to sequentially label cells with molecular barcodes, such that transcripts from each cell are tagged with a unique combination of barcodes; after sequencing, these barcode combinations can then be computationally deconvolved to assign mRNA reads to individual cells. In 2-level sci-RNAseq, cells are permeabilized and fixed before being distributed into individual wells in a 96-well or 384-well plate. The first barcode is added during *in situ* reverse transcription (RT), after which the single-barcoded cells are pooled together and then redistributed via fluorescence-activated cell sorting (FACS) into new 96-well or 384-well plates in limiting numbers. The second barcode is subsequently added during polymerase chain reaction (PCR) amplification on the FACS-sorted cells; individual cells can then be identified by unique combinations of RT barcode and PCR barcode (Cao et al., 2017). 3-level sci-RNAseq relies on the same split-and-pool strategy as 2-level sci-RNAseq, but adds a third level of barcoding, thus greatly increasing the potential throughput; while 2-level sci-RNAseq can capture tens of thousands of cells in an experiment, 3-level sci-RNAseq can capture millions of cells (Cao et al., 2019; Rosenberg et al., 2018).

Chapter 2. MACROPHAGES UNDERGO TRANSIENT POLARIZATION AND REPOLARIZATION IN RESPONSE TO CYTOKINE STIMULATION *IN VITRO*

Chapter 2 is adapted with minimal modification from:

Liu, S.X., Gustafson, H.H., Jackson, D.L., Pun, S.H., and Trapnell, C. (2020) Trajectory analysis quantifies transcriptional plasticity during macrophage polarization. *Scientific Reports*, doi: 10.1038/s41598-020-68766-w.

2.1 ABSTRACT

In recent years, macrophages have been shown to be tremendously plastic in both *in vitro* and *in vivo* settings; however, it remains unclear whether macrophages retain any persistent memory of past polarization states which may then impact their future repolarization to new states. Here, we perform deep transcriptomic profiling at high temporal resolution as macrophages are polarized with cytokines that drive them into “M1” and “M2” molecular states. We find through trajectory analysis of their global transcriptomic profiles that macrophages, which are first polarized to M1 or M2 and then subsequently repolarized, demonstrate little to no memory of their polarization history. We observe complete repolarization both from M1 to M2 and vice versa, and we find that macrophage transcriptional phenotypes are defined by the current cell microenvironment, rather than an amalgamation of past and present states.

2.2 INTRODUCTION

Cellular plasticity broadly refers to cells' ability to assume different phenotypic identities. While cellular plasticity is perhaps best known as a canonical feature of embryonic differentiation in early development, it is also crucial for enabling differentiated cells to respond dynamically to changing microenvironments, as in the case of immune cells redirecting their function in response to different extracellular signals (DuPage and Bluestone, 2016).

Macrophages perform a wide variety of crucial, and sometimes contradictory, functions. While "pro-inflammatory" activities like fighting off infections and "anti-inflammatory" activities like wound-healing traditionally have been attributed to M1 and M2 macrophage subsets, studies of macrophages in both *in vitro* and *in vivo* contexts suggest that macrophages are phenotypically plastic and may shift states in response to environmental changes. Introducing a combination of CpG oligodeoxynucleotides (TLR9 agonist) and anti-interleukin-10 receptor antibody (IL-10 signaling antagonist) to tumor-associated macrophages *in vivo* triggered a phenotypic switch from M2-like to M1-like (Guiducci et al., 2005). Tissue-resident macrophages also display a similar plasticity: peritoneal macrophages that were transferred to the lung adopted a lung-specific phenotype, down-regulating peritoneal macrophage-specific genes and up-regulating lung macrophage-specific genes (Lavin et al., 2014). In addition, treating macrophages with different cytokines sequentially *in vitro* triggered corresponding changes in the expression of canonical murine macrophage markers like iNOS and arginase, as well as changes in the panel of cytokines secreted by the stimulated macrophages (Stout et al., 2005).

Macrophages that have been polarized *in vitro*, reprogrammed *in situ*, or engineered with genome editing tools are a promising avenue for cell-based therapeutics (Suzuki et al., 2014). Macrophage dysfunction has been implicated in a wide array of diseases, including asthma (Kim

et al., 2010; Melgert et al., 2010, 2011), obesity (Kanda et al., 2006; Lumeng et al., 2008; Weisberg et al., 2003; Xu et al., 2003), cancer (Mantovani et al., 2011; Murray and Wynn, 2011; Qian and Pollard, 2010; Sica and Mantovani, 2012; Wynn et al., 2013), and atherosclerosis (Hansson and Hermansson, 2011; Libby et al., 2011; Murray and Wynn, 2011). In many of these cases, macrophages are thought to play a key role in disease pathogenesis and are considered a promising therapeutic target. Phenotypic shifts from M2-like to M1-like, or conversely from M1-like to M2-like, have been linked to disease outcome in cancer and obesity (Duluc et al., 2009; Goubau et al., 2009; Guiducci et al., 2005; Hagemann et al., 2008; Kosteli et al., 2010; Lumeng et al., 2007; Watkins et al., 2009). Moreover, efforts to treat disease by reprogramming macrophages or by transplanting engineered macrophages have shown some success in cancer (Duluc et al., 2009; Goubau et al., 2009; Guiducci et al., 2005; Hagemann et al., 2008; Watkins et al., 2009) and hereditary pulmonary alveolar proteinosis (hPAP) (Suzuki et al., 2014). Thus, developing a better understanding of the molecular mechanisms controlling phenotypic shifts between M1-like and M2-like states could give insight into disease etiology and could lead to the discovery of novel therapeutic targets.

While macrophage plasticity is now well-established, it remains unclear the extent to which macrophages retain any memory of past phenotypic states and whether a cell's history might impact its future response to environmental polarization cues. For instance, a dynamical systems view of cellular differentiation posits that cells undergoing molecular state transitions are "attracted" to specific positions along the continuum of molecular phenotypes they might adopt, and that these "attractors" correspond to classically defined cell types (Huang et al., 2007; Trapnell, 2015). It is conceivable that polarization drives macrophages to such attractor states, resulting in stable and self-sustaining activation. Alternatively, stimulation to M1- or M2-like

states may be transient and entirely dependent on the continuous presence of chemical cues in the microenvironment. Furthermore, it is also unclear whether the mechanism of macrophage plasticity operates on the level of individual cells (each cell undergoing a transition from old to new phenotype) or on the level of cell populations (subpopulations displaying the old phenotype being replaced by subpopulations displaying the new phenotype). *In vitro* models of macrophage polarization offer a controlled setting in which to begin investigating the molecular drivers of cellular phenotypic plasticity. Since we culture macrophages under conditions with little to no cell growth, observed changes in cell phenotype can be attributed to plasticity at the level of individual cells.

Here, we investigate the extent to which macrophages' previous polarization affects their response to subsequent repolarization. To this end, we first polarized murine bone marrow-derived macrophages to M1 and M2 states *in vitro*, then observed polarized macrophage responses to either the removal of extrinsic cytokine stimulation altogether or repolarization to the opposite polarization state via a switch in polarizing cytokines. Both the initial polarization trajectory and the subsequent repolarization were characterized using bulk time-course transcriptomic sequencing. We find that *in vitro* mouse macrophages adopt phenotypes directed primarily by their current microenvironment, irrespective of previous polarization state.

2.3 RESULTS

2.3.1 *Cytokine stimulation drives synchronous and homogenous macrophage polarization* in vitro

In order to measure the full transcriptomic profiles of *in vitro* polarized macrophages, we treated murine bone marrow-derived macrophages (BMDMs) with either interferon-γ (IFN-γ) and

lipopolysaccharide (LPS) to induce an M1 polarization state or interleukin-4 (IL-4) to induce an M2 polarization state. Macrophages were harvested at 1, 2, 4, 6, 12, and 24 hours after the addition of cytokines and profiled using bulk RNA-seq (**Figure 2.1A**). We visualized a global transcriptional "trajectory" of these timepoints using multidimensional scaling (MDS), which showed that macrophages embark on distinct programs of gene regulation upon polarization to M1 or M2 (**Figure 2.1B**). To identify differentially expressed genes (DEGs), we compared the 0h M0 timepoint to each M1 and M2 timepoint using Cuffdiff. As measured by the number of differentially expressed genes, at 24 hours, M1 cytokines elicited a stronger transcriptional response (5,387 genes) than M2 cytokines (2,811 genes) (**Figure 2.2**). These included previously defined M1 (*iNOS*) and M2 (*Arg1*) gene markers (**Figure 2.1C**; **Figure 2.3**), confirming that our *in vitro* polarized macrophages developed distinct and expected M1 and M2 phenotypes.

To globally quantify the transcriptomic differences between M1- and M2-polarized macrophages and unpolarized M0 macrophages, we computed the Jensen-Shannon distance (JSD), a measure commonly used to assess transcriptomic similarity (Trapnell et al., 2010), between each polarized sample and the 0h M0 sample. We then compared these distances to the JSD between the later M0 controls (24h M0, 48h M0, and 96h M0) and 0h M0 (**Figure 2.1D**), which establishes the expected variation between unpolarized, cultured macrophages over the time scale of the experiment. Both M1 and M2 macrophages trend towards equilibrium JSD values which are higher than the JSD between different M0 timepoints, reflecting stable polarized phenotypes that are distinct from the unpolarized control. That M1 macrophages are more distant from M0 than M2 cells are by this measure is consistent with the greater number of DEGs between M1 and M0 than between M2 and M0.

In principle, cytokines could elicit heterogeneous or asynchronous responses in individual macrophages, so we analyzed a subset of these timepoints with single-cell transcriptome sequencing. M1- and M2- polarized macrophages formed coherent clusters that were clearly separated from each other and unpolarized cells, with no intermixing of cells from different time points, suggesting that this *in vitro* system drives macrophage polarization in a largely synchronous and homogeneous manner (**Figure 2.4A**). The *in vitro* cultured macrophages also exhibited very low expression of proliferation markers, particularly in the M1 condition, suggesting a low level of cell growth (**Figure 2.4B-C**).

2.3.2 *Polarized macrophages return to baseline upon removal of extrinsic cytokines*

We then wished to explore whether M1- and M2-polarized macrophages could maintain their polarized phenotypes in the absence of extrinsic cytokines in the media, or whether M1 and M2 macrophages would revert back to an unpolarized state without continuous external cytokine stimulation. To investigate this question, M1- and M2-polarized macrophages were washed and then returned to a basic media without any polarizing cytokines (**Figure 2.5A**). Separately, we maintained M1 and M2 macrophages in culture with the original polarizing cytokines as a control. In the absence of continued cytokine exposure, we found that previously polarized macrophages quickly revert to a state that resembles the baseline unpolarized phenotype, in terms of both the expression of individual M1/M2 polarization marker genes and the cells' overall transcriptomes (**Figure 2.5B-C**). After 72h in cytokine-free media, we detected 2,307 differentially expressed genes between M1→M0 macrophages and 0h M0 macrophages (as compared to 4,732 DEGs for the 72h M1 control) and 2,038 differentially expressed genes between M2→M0 macrophages and 0h M0 macrophages (as compared to 3,824 DEGS for the 72h M2 control) (**Figure 2.6**). JSD

between depolarizing M1 and M2 macrophages and 0h M0 also trends down towards the baseline JSD value between different M0 timepoints (**Figure 2.5D**). Most M1 and M2 marker genes returned to levels very similar to the M0 cells, although there were some exceptions. For example, following removal of M1 cytokines, while *Tnf* was reduced to 36.7% of its peak expression levels and 62.7% of equilibrium 96h M1 levels, *Tnf* expression remained slightly elevated relative to M0 cells at 96 hours (**Figure 2.7A**). Similarly, while *Retnla* expression levels drop to 55% of their 24h M2 levels in 96h M2→M0 cells, the gene is still expressed at higher levels than in M0 cells (**Figure 2.7B**). These results suggest that most genes upregulated as part of M1 or M2 polarization do not remain expressed at maximal levels in the absence of extrinsic cytokine stimulation, often returning to their pre-polarization levels.

2.3.3 *Polarized macrophages exposed to new cytokines undergo repolarization to a new phenotype*

Given that previously polarized macrophages largely revert to an unpolarized state when external cytokine stimuli are removed, we wished to explore how polarized macrophages would respond when exposed to a new cytokine stimulus. To investigate how macrophages respond to a switch in polarizing cytokines, macrophages which were initially cultured with IFN-γ + LPS to induce an M1 state were washed to remove the original cytokines and then cultured with IL-4, and vice versa (**Figure 2.8A**).

Macrophages that experienced a switch in cytokine stimuli adopted a polarized phenotype corresponding to the new cytokine treatment, displaying a similar phenotypic plasticity to the depolarized macrophages. Macrophages first polarized to an M2 state with IL-4, then subsequently repolarized with IFN-γ + LPS to an M1 state exhibit marker gene expression patterns and global

transcriptomes typical of M1-polarized macrophages, and vice versa (**Figure 2.8B-C)**. Of the 4,732 genes differentially expressed between M1-polarized and M0 macrophages, 76% are also differentially expressed between M2→M1 repolarized macrophages and M0 macrophages (**Figure 2.2**; **Figure 2.9A**; **Figure 2.10**). In contrast, 1,300 genes are differentially expressed between M1 and M2→M1 macrophages, and the majority of these DEGs were less than two-fold up- or down-regulated (**Figure 2.9B**). In cells previously polarized to M2, canonical M1 genes *Myd88*, *Nfkb1*, and *Tnf* all equilibrated to levels similar to that of cells maintained in M1 conditions throughout the experiment (**Figure 2.11A**).

Repolarizing M1 macrophages with M2 cytokines revealed a similar pattern: of 3,824 genes differentially expressed between M2-polarized and M0 macrophages, 58% are also differentially expressed between M1→M2 repolarized macrophages and M0 macrophages, and 2,225 genes are differentially expressed between M2 and M1→M2 macrophages, with similarly modest fold changes (**Figure 2.9B**). 72 hours after the media switch, M2 marker genes *Pparg*, *Retnla*, and *Stat6* were all expressed at similar levels in M1→M2 cells compared to macrophages maintained in M2 conditions (**Figure 2.11B**). In terms of JSD, the distance between M2→M1 repolarized macrophages and 24h M1-polarized macrophages decreases over time as repolarized macrophages adopt more M1 characteristics; similarly, the distance between M1→M2 macrophages and 24h M2-polarized macrophages also decreases over time as those macrophages take on more M2 characteristics, although 72 hours was not sufficient to completely adopt the M2 transcriptomic profile (**Figure 2.8D**). Taken together, these results suggest that macrophage transcriptomic phenotypes are highly plastic, regulating most genes to reflect their current signaling environment with minimal residual transcriptional “memory”.

2.3.4 *Polarized macrophages exhibit plasticity in chromatin accessibility*

Since our RNA-seq data suggested that macrophage transcriptomes transiently reflect the cells' current environment, we wished to investigate whether macrophage chromatin accessibility would also be similarly plastic. To this end, we collected bulk ATAC-seq data for three conditions: an unpolarized control (0h M0), a M1-polarized sample (IFN-γ + LPS for 24h), and a depolarized M1→M0 sample (IFN-γ + LPS for 24h, then basic media for 72h) (**Figure 2.12A**). Of 8,749 differentially accessible sites between unpolarized (M0) and M1-polarized macrophages, 47% (4,122 sites) remain differentially accessible between depolarized M1 and M0 macrophages. However, the Jensen-Shannon distance (JSD) between the global chromatin profiles of depolarized M1 macrophages and M0 macrophages was comparable to the JSD between the M0 replicates to one another, suggesting that macrophage chromatin profiles, by in large, revert to a baseline unpolarized state in the absence of extrinsic stimulation and recapitulating trends seen for the transcriptome (**Figure 2.12B**). The median (absolute) log-fold change in differentially accessible sites between depolarized M1 macrophages and M0 macrophages (1.03) was also lower than the median log-fold change between M1 macrophages and M0 macrophages (1.42), indicating that both the number of differentially accessible sites and the magnitude of the accessibility differences at these sites are decreasing as macrophages depolarize (**Figure 2.12C**). Finally, the log fold-change of chromatin accessibility between M1-polarized macrophages and M0 macrophages is closely correlated with the log fold-change of accessibility between M1-polarized macrophages and M1→M0 macrophages, suggesting that the chromatin accessibility profiles of M0 and M1→M0 macrophages are broadly similar, despite the presence of differentially accessible sites (**Figure 2.12D**). Looking specifically at sites falling within 500bp of a gene transcription start site, there does exist a subset of gene-associated sites that remain accessible in

M1→M0 macrophages compared to M0. Of the 10 genes that are four-fold more accessible in M1→M0 compared to M0, all 10 are also four-fold more accessible in M1 compared to M0 (in total, 132 genes were four-fold more accessible in M1 vs. M0; Fisher's overlapping p-value = 2.7e-23). Two of these genes are detectably expressed in the bulk RNA-seq timecourse data, but neither exhibits a pattern of upregulated expression in M1 and M1→M0 (**Figure 2.13**).

2.4 DISCUSSION

Previous studies have established that macrophages are sensitive to changes in their local microenvironment and display a high level of phenotypic plasticity both *in vitro* and *in vivo* (Guiducci et al., 2005; Lavin et al., 2014; Stout et al., 2005). However, it has remained unclear whether macrophages' past polarization history left any memory that could impact subsequent repolarization, and whether macrophages, once polarized, could maintain their polarized phenotype without continued extrinsic signals. In this study, we have performed high-resolution transcriptomic profiling of macrophages through polarization to M1 and M2 and then subsequent repolarization (cytokine switch) and depolarization (removal of all polarizing cytokines). These experiments demonstrated that macrophages' global molecular phenotypes are primarily dependent on the current microenvironment, with little to no memory of past polarization states. Upon initially polarizing cells with M1- or M2-inducing cytokines, they underwent dramatic transcriptional change, traversing a trajectory characterized by the regulation of thousands of genes. However, these molecular phenotypes were transient; upon removal of extrinsic polarizing cytokines, previously polarized macrophages reverted to a baseline state comparable to the unpolarized control, suggesting that continuous external stimulation is required to maintain a polarized macrophage phenotype. Furthermore, we observed extensive repolarization from both

M1 to M2 and M2 to M1, suggesting that macrophages may move freely along the phenotypic spectrum between M1 and M2 states. Analysis of chromatin accessibility profiles for M1-polarized and subsequently depolarized macrophages also shows almost complete reversion to baseline. Most marker genes classically associated with the M1 and M2 phenotypes were expressed at levels that reflected current rather than past signaling, although there were a few genes that had not equilibrated to the levels observed in cells maintained in M1 or M2 cytokines, consistent with a previous study that looked only at such markers (Smith et al., 2016). Regardless, Smith *et al*. concluded that a relatively simple regulatory network comprised of feedforward loops to stabilize the M1 and M2 programs and mutual inhibition between them was insufficient to adequately explain their data. Our observations reinforce that conclusion and suggest that the signals tested here, which are classically associated with M1 and M2 macrophage phenotypes, are not sufficient to push cells into stable molecular "attractor" states.

We designed these experiments to maximize the chance of detecting molecular "hysteresis" by using deep transcriptome sequencing with finely resolved temporal sampling under highly controlled conditions. However, there are several important caveats to this design. First, macrophages were treated with high doses of polarizing cytokines; while high doses were used in order to generate a robust polarization response, they may also be responsible for the rapidness of the observed polarization and the lack of asynchronicity between individual cells. The concerted, rapidly transient response we see here may not accurately reflect the responses of macrophages *in vivo*, where cells could be exposed to a wide array of (potentially conflicting) signals and over a range of doses. Second, these *in vitro* experiments exclude many co-stimulatory molecules present in the *in vivo* milieu that, while not classically associated with M1 or M2 phenotypes, may nevertheless stabilize them. Third, it is possible that longer exposure times or alternate doses of

these cytokines might elevate cells above a critical threshold of polarization required for hysteresis. Fourth, bone-marrow derived and tissue resident macrophages vary in their response to inflammatory cytokines, so the results observed in this study may not be applicable to tissue resident macrophages. Finally, macrophage polarization varies across genetic background, and macrophages derived from other mouse strains might exhibit different polarization kinetics and potentially attenuated repolarization (Buscher et al., 2017).

The transience of polarized macrophage phenotypes has implications for potential therapies that rely on reprogramming macrophages. Stabilizing a desired macrophage phenotype may require that cells be continuously exposed to a particular combination of signals or engineered to constitutively activate pathways downstream of those signals. Maintaining a particular signaling milieu *in vivo* is likely to be challenging after macrophage transplantation, and engineering cells (e.g. with genome editing) carries risks. Nevertheless, understanding the molecular machinery that endows macrophages with such plasticity remains an important goal. That macrophages are so responsive to their current signaling environment suggests that future efforts to dissect macrophage signaling pathways with tissue- and context-specific cues could be very fruitful, both for basic immunology and for clinical applications.

2.5 MATERIALS AND METHODS

2.5.1 *Mice*

Wild-type C57BL/6J 6 to 10 week-old mice were obtained from Jackson Laboratory. All experiments were approved by the Institutional Review Board (IACUC, University of Washington) and were performed in accordance with relevant guidelines and regulations.

2.5.2 *Macrophage cell culture*

Mice were killed by cervical dislocation, and bone marrow cells were harvested by flushing femur bones with RPMI-1640. Bone marrow cells were plated at a concentration of 6 x 10^6 cells per 3 cm petri dish, then cultured in a base media of RPMI-1640 with 20% horse serum, 100 U/mL penicillin, 100 μg/mL streptomycin, and 20 ng/mL macrophage colony stimulating factor (MCSF). On day 7, cells were stimulated with 100 ng/mL LPS and 25 ng/mL interferon-γ (IFN-γ) or 25 ng/mL interleukin-4 (IL-4) to induce polarization to M1 or M2 states, respectively, or maintained in base media as a control. For repolarization, bone marrow-derived macrophages (BMDMs) were primed with LPS + IFN-γ or IL-4 for 24h, washed with PBS, then either treated with the opposing stimulus, maintained in the original stimulus, or returned to base media. Samples were collected for bulk RNA-seq analysis 1h, 2h, 4h, 6h, 12h, and 24h post-treatment for polarization, and 1h, 2h, 4h, 6h, 12h, 24h, and 72h post-treatment for repolarization. Three biological replicates were collected for the full set of polarization and repolarization conditions. For single cell RNA-seq, a single replicate was collected in which cells were harvested and cultured as described above for a subset of polarization conditions: 0h M0, 6h M0, 24h M0, 6h M1, 24h M1, 6h M2, and 24h M2. For bulk ATAC-seq, cells were also harvested and cultured as described above for three biological replicates of the following conditions: 0h M0, 24h M1, and 72h M1→M0.

2.5.3 *Sample collection and library preparation*

Samples were harvested by removing the media, then adding trizol directly to the macrophages in the culture plates. Bulk RNA was isolated from the trizol solution via phenol extraction. cDNA synthesis and enrichment were performed using Illumina TruSeq v2 kits on 500 ng total RNA for each sample. ERCC spike-in RNA (Ambion) was added to the total RNA at a

final dilution of 1:5,000 according to the ThermoFisher guidelines (1uL of 1:100 ERCC dilution added to 500ng of total RNA in a total volume of 50uL). The libraries were sequenced on the Illumina NextSeq 500 platform using a v2 75-cycle kit (Read 1: 35 cycles, Read 2: 35 cycles, Index 1: 6 cycles). Bulk ATAC libraries were prepared using the Greenleaf protocol (Buenrostro et al., 2015) and sequenced on the Illumina NextSeq 500 platform using a v2 75-cycle kit (Read 1: 35 cycles, Read 2: 35 cycles, Index 1: 10 cycles, Index 2: 10 cycles).

For single cell RNA-seq, samples were collected by removing media, washing with PBS, then incubating with 3 mL cold Versene for 5 minutes on ice. Macrophages were then harvested by scraping the plates. Single cell RNA-seq libraries were generated using 10X v1 and sequenced on the Illumina NextSeq 500 platform using a v2 75-cycle kit (Read1: 98 cycles, Read 2: 10 cycles, Index 1: 14 cycles, Index 2: 8 cycles).

2.5.4 *Read alignments and construction of the expression matrices*

Base calls were converted to fastq format and demultiplexed using Illumina's bcl2fastq/2.16.0.10. Demultiplexed reads were aligned to the mouse reference genome (mm10) using Tophat v2.0.14 with default settings (Kim et al., 2013). For the RNA-seq data, aligned reads were quantified using Cuffquant v2.2.2, and then a normalized gene expression matrix was generated using Cuffnorm v2.2.2 (Roberts et al., 2011a, 2011b; Trapnell et al., 2010, 2013). For the ATAC-seq data, PCR duplicates were removed using Samtools v1.9 (Li et al., 2009), and data from all alignment files were merged into a single file for peak calling using MACS v2.1.0 (parameters: --nomodel --keep-dup all --extsize 200 --shift -100 -B --SPMR --call-summits) to generate a master list of peaks observed in the experiment (Zhang et al., 2008). A peak count matrix was calculated by using Bedtools v2.28.0 (Quinlan and Hall, 2010) to compute the

intersection between each sample's aligned reads and the master list of peaks. Expression matrices for the single cell data were generated using the 10X Cell Ranger pipeline (10X Genomics).

2.5.5 *RNA-seq analysis*

The normalized gene expression matrix was loaded into R (v3.4.0) and filtered to include only genes with at least 10 FPKM in at least 1 sample. Multidimensional scaling coordinates were computed based on the average expression values (mean across three replicates) for each sample. Jensen Shannon distances (JSDs) were computed between each treatment condition and the 0h M0 control using proxy v0.4-17 (R Core Team, 2018). Differential gene expression was calculated using Cuffdiff v2.2.2 (Trapnell et al., 2013).

For the single cell data, the normalized gene expression matrix was loaded into R (v3.5.2) (R Core Team, 2018) and analyzed using Monocle 3 beta (v0.1.2) (Qiu et al., 2017; Trapnell et al., 2014). To generate the UMAP plot, data normalization and preprocessing were run with the default parameter settings, dimensionality reduction and cell clustering were run using the UMAP reduction method option (Becht et al., 2018), and graph learning was run using learn_graph_control = list(ncenter=1000), and default settings otherwise. Proliferation scores were computed as log10(aggregate_marker_expression), where aggregate marker expression was calculated as the sum of size factor-corrected expression for a panel of cell proliferation marker genes (listed in **Figure 2.4C**). Figures were generated using ggplot2 (Wickham, 2009).

2.5.6 *ATAC-seq analysis*

The raw peak count was loaded into R (v3.4.0) (R Core Team, 2018) and normalized using DESeq2 v1.10.1 (Love et al., 2014), then filtered to include only peaks with greater than 10 counts in at least 1 sample. Differentially accessible peaks were also calculated using DESeq2. Sites were considered to be associated with a gene if they were located within 500 bp of a gene's transcription start site. Using proxy v0.4-17 (R Core Team, 2018), Jensen Shannon distances (JSDs) were calculated between the three replicates of the baseline condition (0h M0) and between each of the replicates for each of the treatment conditions (24h M1 and 72h M1→M0) and each of the 0h M0 replicates. Final JSD values for each treatment condition were computed as the average of JSDs for all unique pairs between the three replicates of each treatment condition and the three replicates of the 0h M0 control. Figures were generated using ggplot2 (Wickham, 2009).

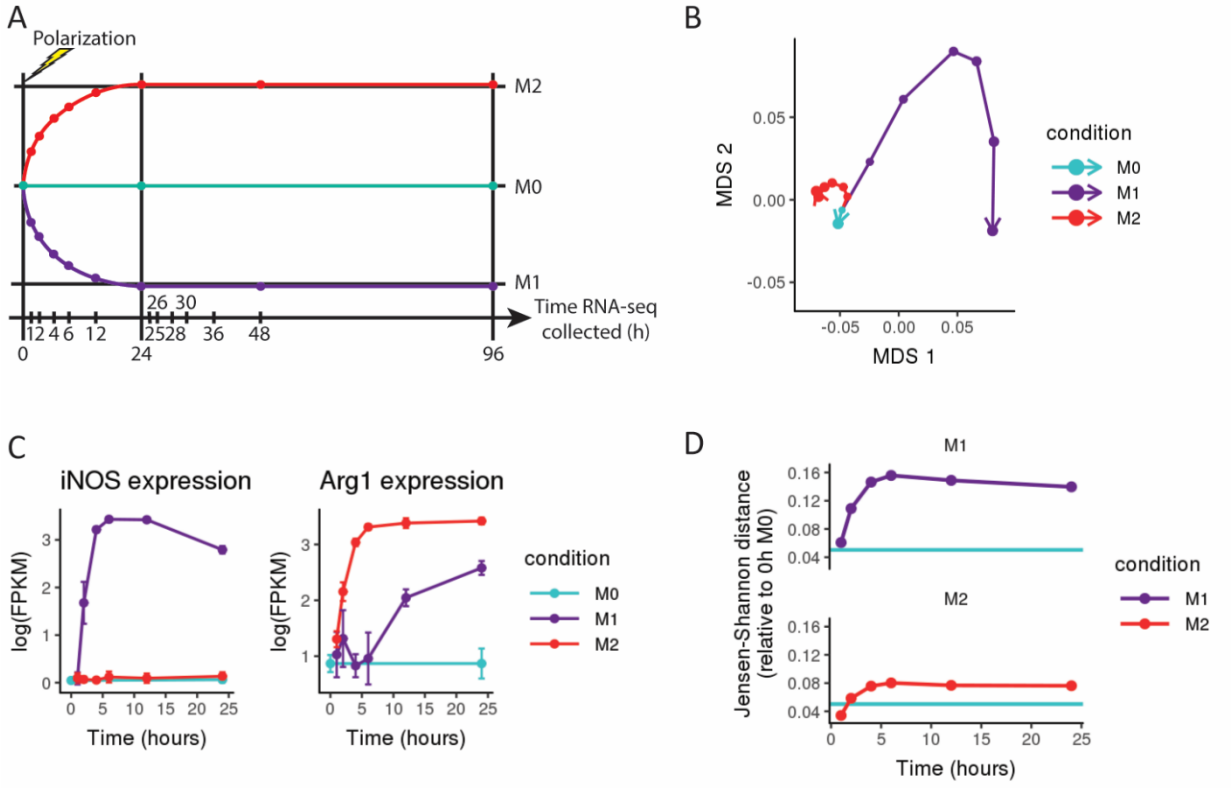

Figure 2.1: *In vitro* polarized macrophages display distinct M1 and M2 phenotypes.

A) Schematic of experimental design, where each point represents a collected sample, and each colored trajectory represents a different treatment condition. Murine bone marrow-derived macrophages were treated with cytokines to induce polarization (IFN-γ + LPS for M1, IL-4 for M2); M0 was maintained in base media as an unpolarized control (n = 3). B) Multidimensional scaling (MDS) plot of RNA-seq expression (averaged across three replicates for each sample); points representing each sample are connected in order of collection, with point size representing the time spent (in hours) in culture. Macrophages treated with IFN-γ + LPS (M1) and IL-4 (M2) follow distinct polarization trajectories. C) Gene expression in log(FPKM) of *iNOS* (a marker gene for M1 polarization) and *Arg1* (a marker gene for M2 polarization) over time. D) Jensen-Shannon distance (JSD) between the RNA expression profiles of M1- and M2-polarized macrophages and the 0h M0 control. As a baseline for expected global expression differences between samples, the teal line shows the average JSD between all later M0 controls (collected at 24h, 48h, and 96h) and the original 0h M0 control sample.

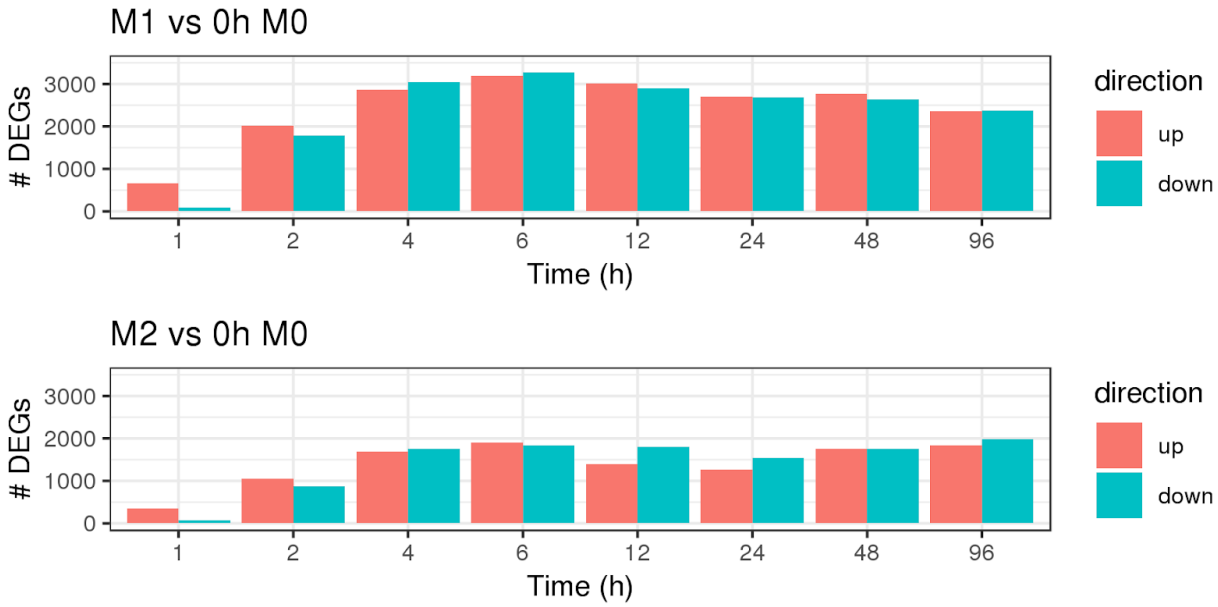

Figure 2.2: Differentially expressed genes for M1 and M2 compared to 0h M0.

Bar plot of the number of differentially expressed genes (up-regulated and down-regulated) with q-value < 0.05 for each M1 and M2 timepoint compared to the 0h M0 condition (n = 3).

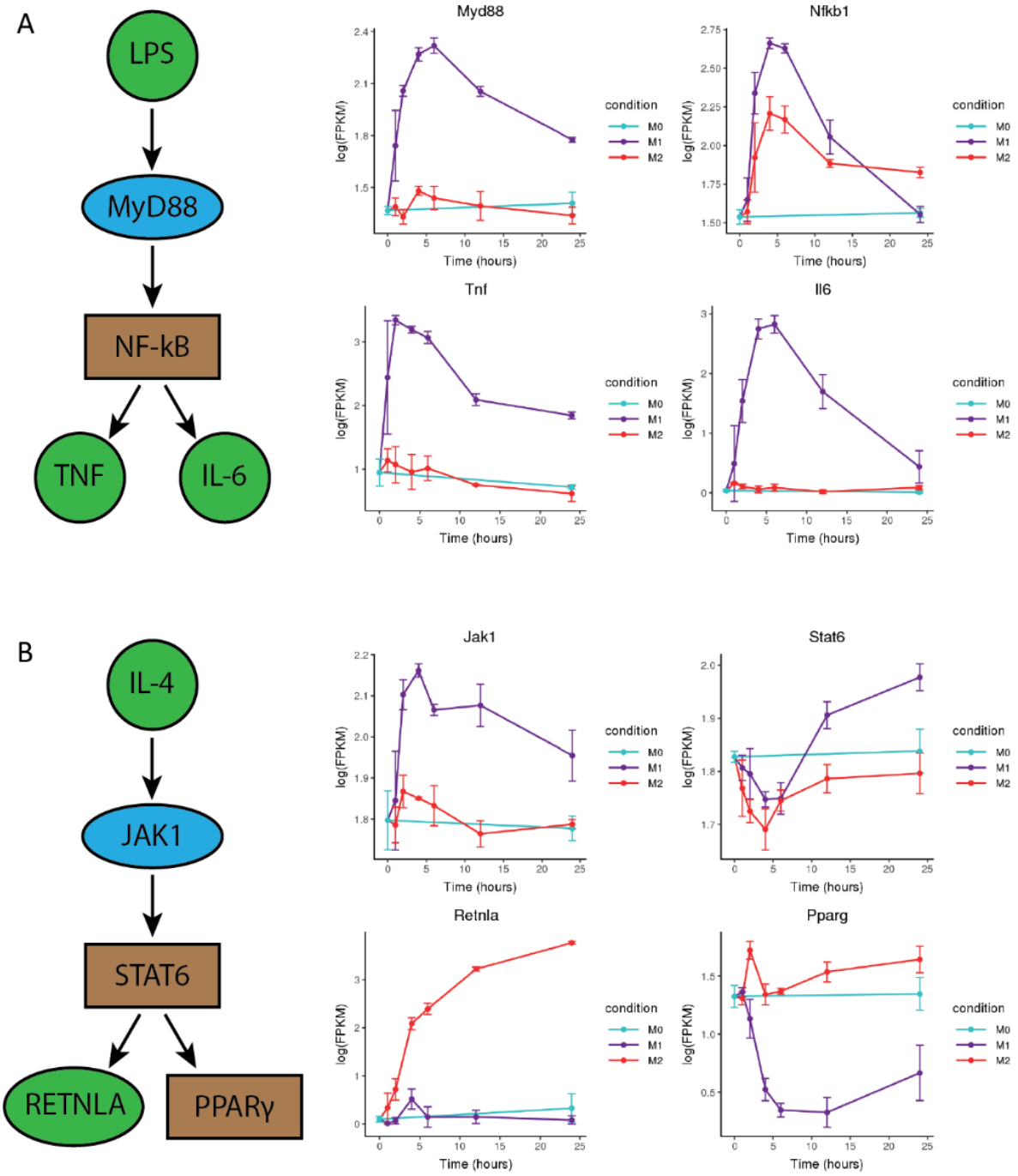

Figure 2.3: Gene expression of key M1 and M2 marker genes during polarization.

A) Schematic of a simplified M1 polarization signaling pathway, highlighting key marker genes (left) and plots of the expression of these marker genes over time during macrophage polarization (right). B) Schematic of a simplified M2 polarization signaling pathway, highlighting key marker genes (left) and plots of the expression of these markers over time during macrophage polarization (right). Some genes, such as *Nfkb1* and *Jak1*, are active in both M1 and M2 polarization, leading to some overlap in expression patterns. Three biological replicates were analyzed for each timepoint.

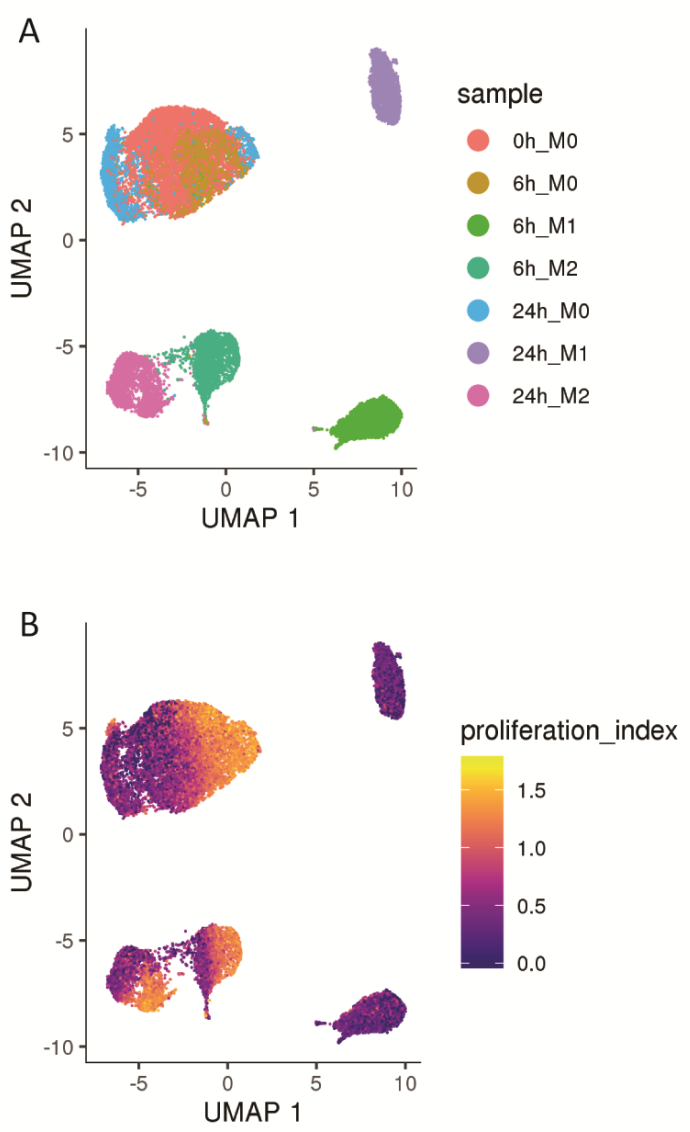

C

Proliferation Markers		
Rpa2	Cks1b	Pcna
Ung	Kif20b	Casp8ap2
Pola1	Kif2c	Rfc2
Blm	Gtse1	Dtl
Gins2	Anln	Gas2l3
Rrm2	Ckap2	Nek2
Cdc45	Cdca3	Hjurp
Gmnn	Cks2	Cenpf
Ccne2	Cdc25c	Ube2c
E2f8	Hmgb2	Birc
Tipin	Rangap1	Aurkb
Brip1	Kif11	Smc4
Mcm4	Anp32e	Cenpa
Dscc1	Ctcf	Cdca8
Cdca7	Kif23	Tubb4b
Mcm6	G2e3	Dlgap5
Mcm5	Bub1	Ect2
Hells	Lbr	Cdk1
Rad51	Mki67	Top2a
Msh2	Ccnb2	Tpx25
Nasp	Ckap2l	Cbx5
Rad51ap1	Nuf2	Tacc3
Wdr76	Ttk	Ncapd2
Fen1	Hmmr	Cdca2
Prim1	Ckap5	Psrc1
Tyms	Tmpo	Usp1
Ubr7	Cenpe	Rrm1
Chaf1b	Nusap1	Clspn
Exo1	Ndc80	Uhrf1
Cdc6	Aurka	Slbp
Mcm2	Cdc20	

Figure 2.4: *In vitro* polarized macrophages display distinct M1 and M2 phenotypes and synchronous progression.

Murine bone marrow-derived macrophages were treated with cytokines to induce polarization (IFN-γ + LPS for M1, IL-4 for M2); M0 was maintained in base media as an unpolarized control (n = 1). A) Macrophages treated with IFN-γ + LPS (M1) and IL-4 (M2) follow distinct polarization trajectories. M1- and M2-polarized macrophages also form distinct clusters by timepoint, showing very little intermixing. B) Cultured BMDMs exhibit low expression of proliferation markers; expression in M1-polarized macrophages is particularly low. Proliferation index is computed as log10(aggregate_proliferation_marker_expression), where aggregate marker expression is calculated as the sum of size factor-corrected marker gene expression for each cell. C) List of the proliferation markers used to compute the proliferation index.

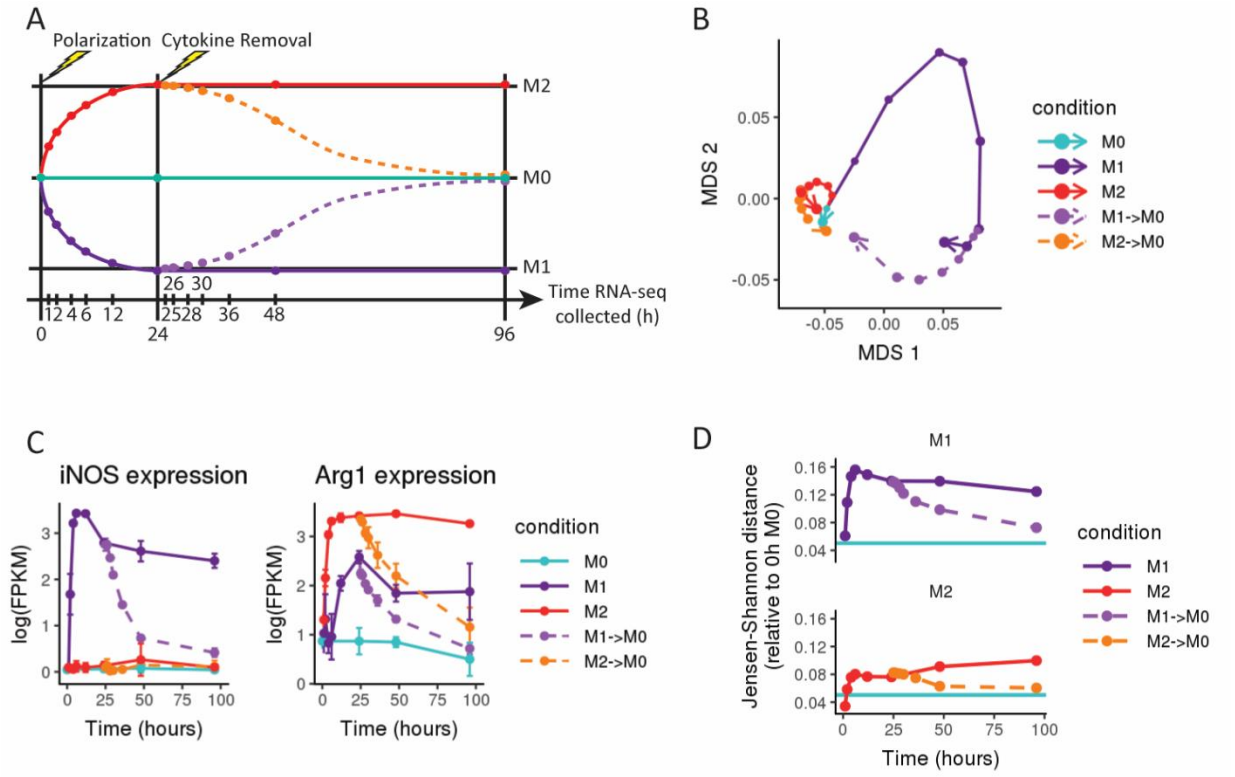

Figure 2.5: Polarized macrophage phenotypes are transient.

A) Schematic of experimental design, where each point represents a collected sample, and each colored trajectory represents a different treatment condition. Murine bone marrow-derived macrophages were treated with cytokines to induce polarization (IFN-γ + LPS for M1, IL-4 for M2); M0 was maintained in base media as an unpolarized control. After 24 hours, cells were washed to remove cytokines and then cultured in base media with no polarizing cytokines (n = 3). B) Multidimensional scaling (MDS) plot of RNA-seq expression (averaged across three replicates for each sample); points representing each sample are connected in order of collection, with point size representing the time spent (in hours) in culture. After the removal of polarizing cytokines, the expression profiles of previously polarized macrophages follow trajectories that trend towards the M0 baseline. C) Gene expression in log(FPKM) of *iNOS* (a M1 marker gene) and *Arg1* (a M2 marker gene) over time. While marker gene expression increases with initial polarization, it drops sharply upon the removal of polarizing cytokines and falls to near baseline levels after 72h in base media. D) Jensen-Shannon distance (JSD) between the RNA expression profiles of polarized and depolarized macrophages compared to the 0h M0 control. As a baseline for expected global expression differences between samples, the teal line shows the average JSD between all later M0 controls (collected at 24h, 48h, and 96h) and the original 0h M0 control sample. While JSD initially increases as polarizing macrophages develop distinct mRNA expression profiles and diverge from the unpolarized baseline, removal of polarizing cytokines triggers a reversion towards the baseline.

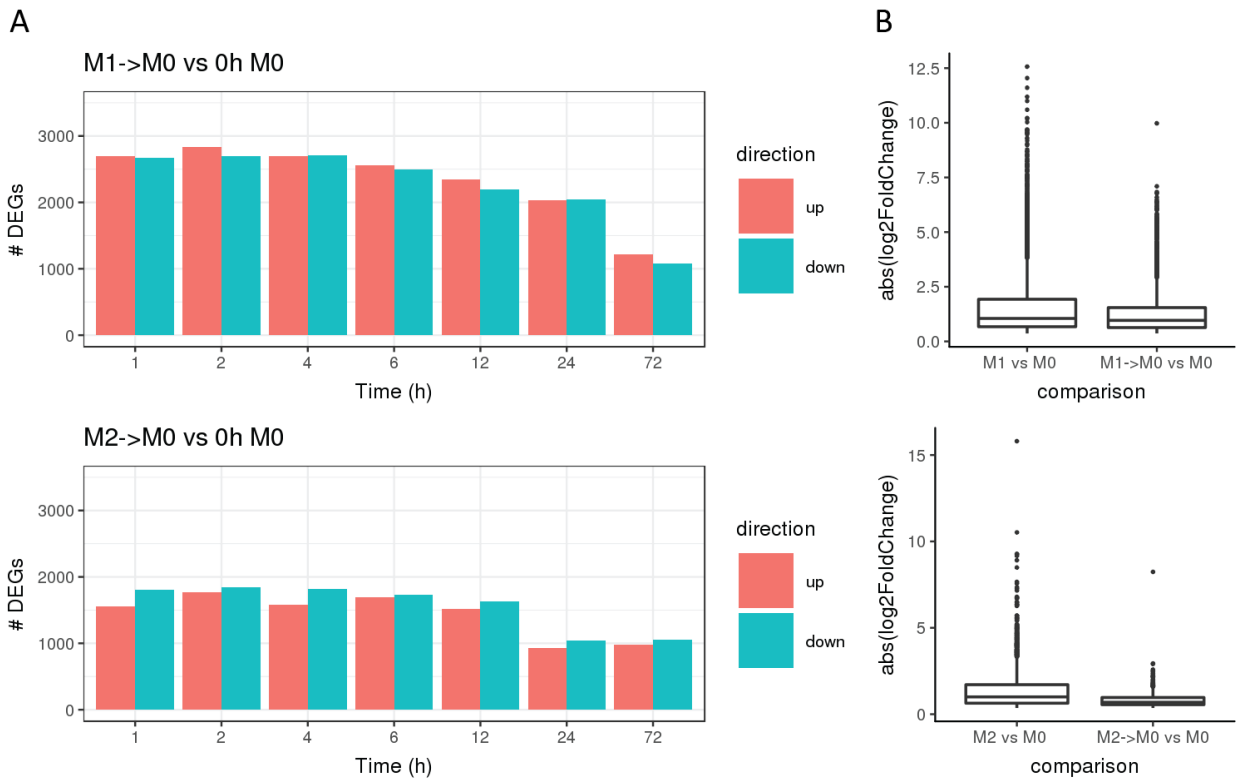

Figure 2.6: Differentially expressed genes for M1→M0 and M2→M0 compared to 0h M0 and 96h M0.

A) Bar plot of the number of differentially expressed genes (up-regulated and down-regulated) with q-value < 0.05 for each M1→M0 and M2→M0 timepoint compared to the 0h M0 condition (n = 3). B) Box plots of the absolute log2 fold change in gene expression of 96h M1 and 72h M1→M0 compared to 96h M0 (top) and 96h M2 and 72h M2→M0 compared to 96h M0 (bottom).

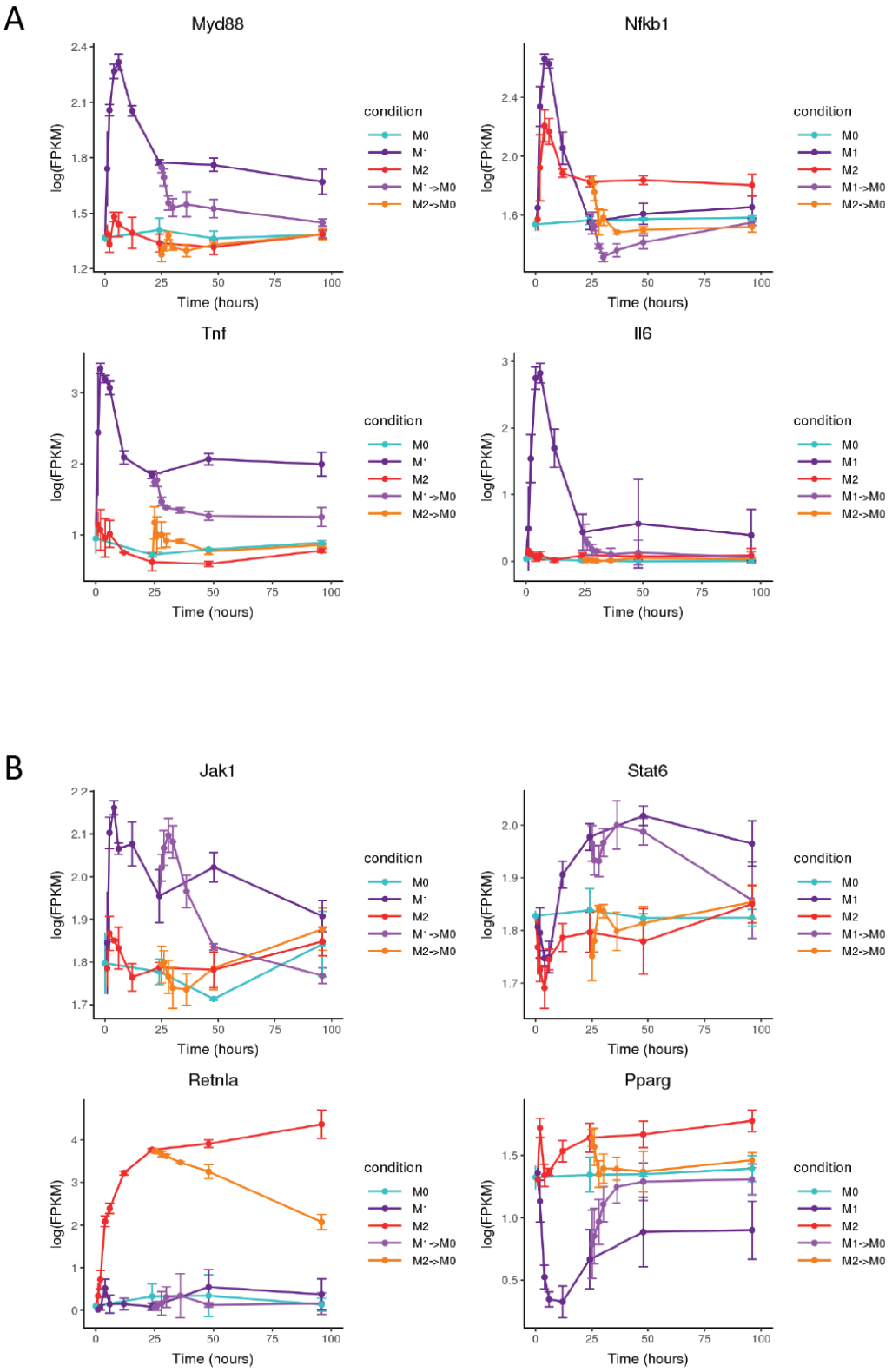

Figure 2.7: Gene expression of key M1 and M2 marker genes during polarization and depolarization.
(*legend continued on next page*)

Figure 2.7: (*continued*) A) Plots of the expression of M1 marker genes over time during macrophage polarization and subsequent depolarization (n = 3). B) Plots of the expression of M2 marker genes over time during macrophage polarization and subsequent depolarization (n = 3). Some genes, such as *Nfkb1* and *Jak1*, are active in both M1 and M2 polarization, leading to some overlap in expression patterns.

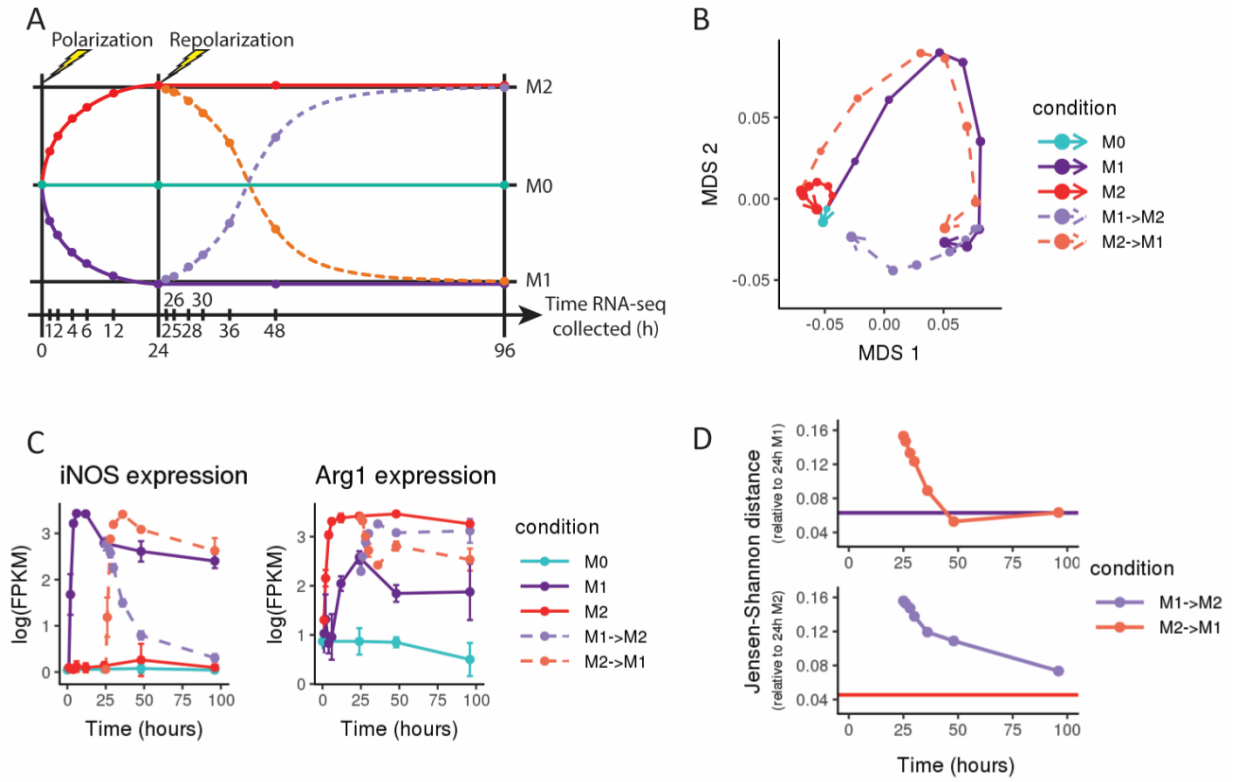

Figure 2.8: Macrophages convert between polarized states in response to cytokine treatment.

A) Schematic of experimental design, where each point represents a collected sample, and each colored trajectory represents a different treatment condition. Murine bone marrow-derived macrophages were treated with cytokines to induce polarization (IFN-γ + LPS for M1, IL-4 for M2); M0 was maintained in base media as an unpolarized control. After 24 hours, cells were washed to remove cytokines and then cultured with the alternate set of polarizing cytokines (M1 switched to M2, and vice versa) (n = 3). B) Multidimensional scaling (MDS) plot of RNA-seq expression (averaged across three replicates for each sample); points representing each sample are connected in order of collection, with point size representing the time spent (in hours) in culture. After switching polarizing cytokines, the expression profiles of previously polarized macrophages follow trajectories that trend towards the new polarized state. C) Gene expression in log(FPKM) of *iNOS* (a M1 marker gene) and *Arg1* (a M2 marker gene) over time. Switching the polarizing cytokines induces reduced expression of the previous marker gene and increased expression of the marker associated with the new polarization state. D) Jensen-Shannon distance (JSD) between the RNA expression profiles of M2→M1 repolarized macrophages compared to 24h M1-polarized macrophages (top) and M1→M2 macrophages compared to 24h M2-polarized macrophages (bottom). As a baseline for expected global expression differences between M1-polarized samples over time, the purple line in the top panel shows the average JSD between both later M1 controls (collected at 48h and 96h) and the 24h M1 sample. Similarly, the red line in the bottom panel shows the average JSD between both later M2 controls (48h and 96h) and the 24h M2 sample. After switching media, the JSD for repolarized macrophages decreases as M1→M2 macrophages become more similar to M2-polarized macrophages and M2→M1 macrophages become more similar to M1-polarized macrophages.

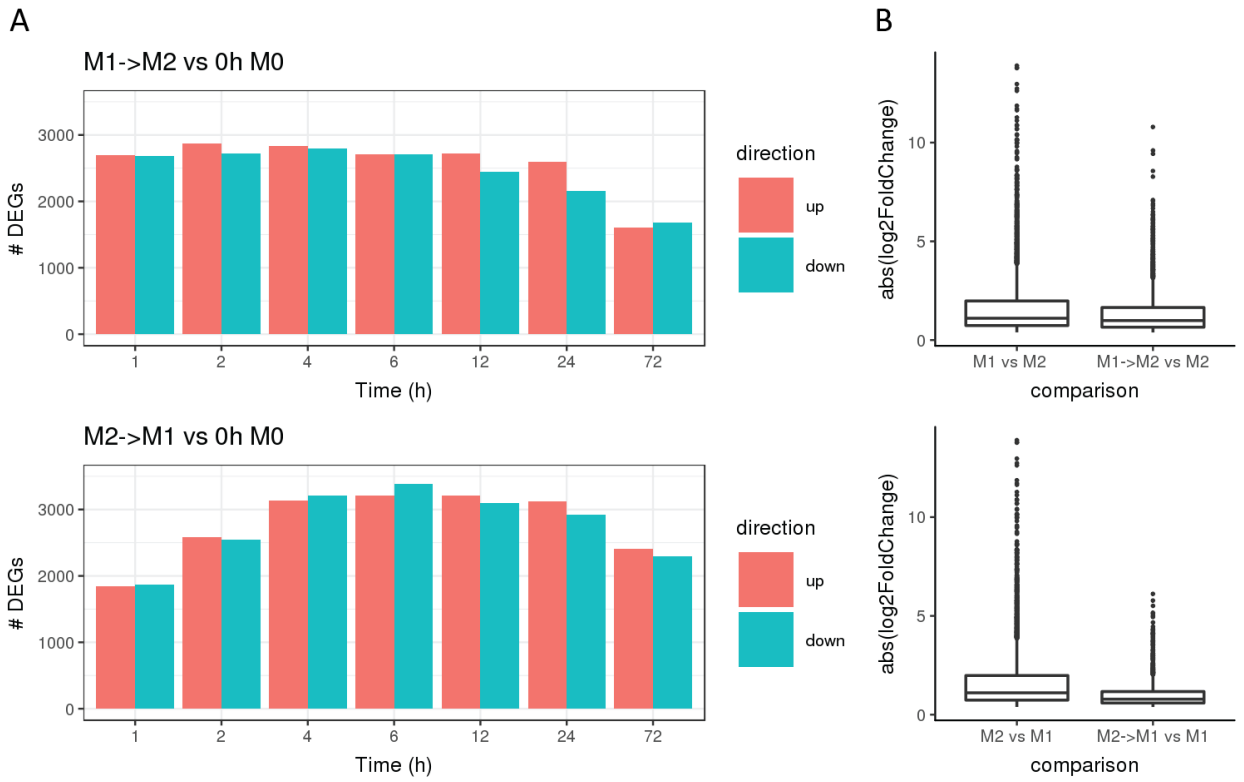

Figure 2.9: Differentially expressed genes for M1→M2 and M2→M1 compared to 0h M0 and 96h M1 and M2.

A) Bar plot of the number of differentially expressed genes (up-regulated and down-regulated) with q-value < 0.05 for each M1→M2 and M2→M1 timepoint compared to the 0h M0 condition (n = 3). B) Box plots of the absolute log2 fold change in gene expression of 96h M1 and 72h M1→M2 compared to 96h M2 (top) and 96h M2 and 72h M2→M1 compared to 96h M1 (bottom).

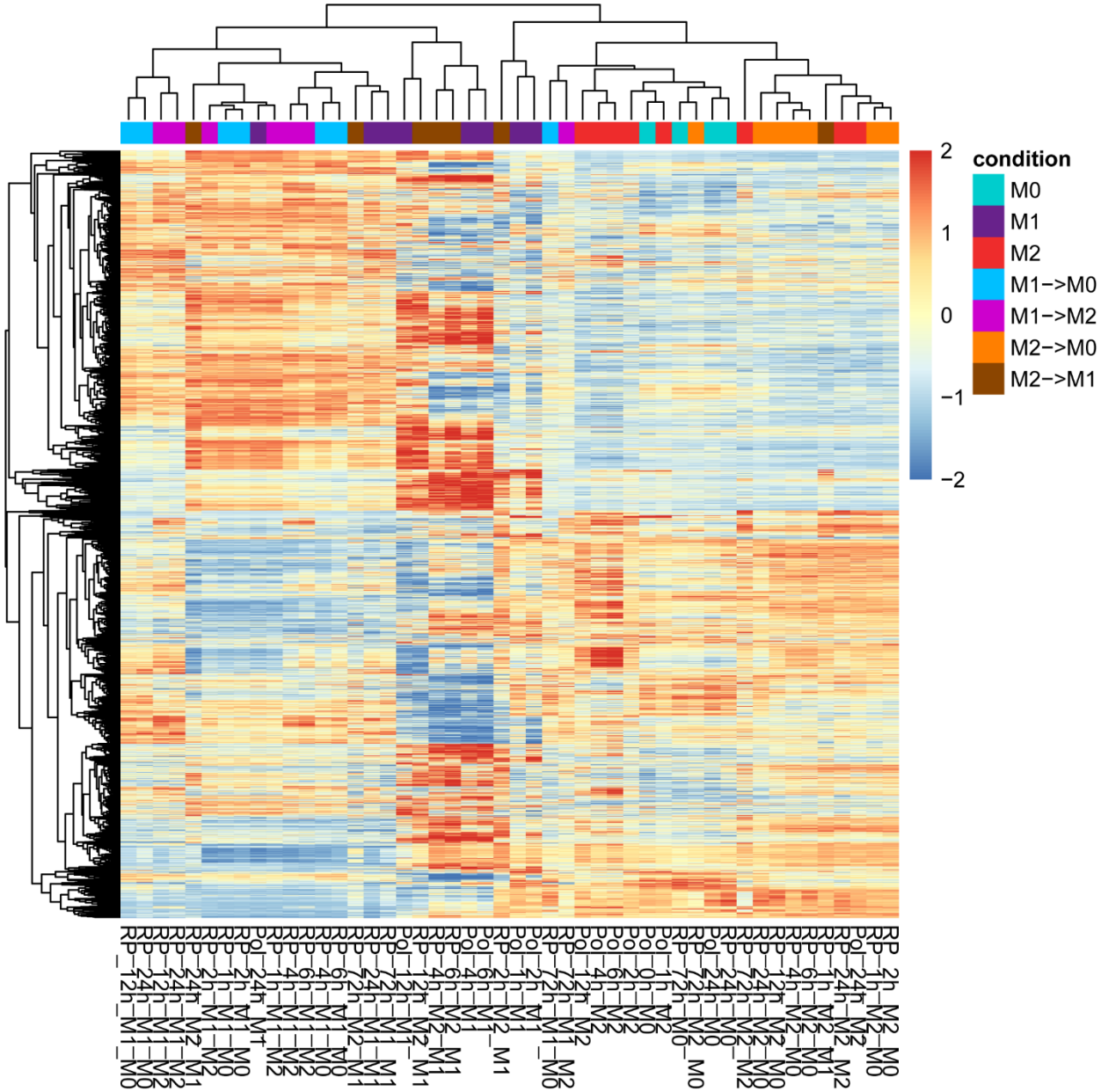

Figure 2.10: Heatmap of differentially expressed genes.

Heatmap of genes differentially expressed between at least one condition and 0h M0 condition with q-value < 0.05, and expressed at a level of >= 10 FPKM in at least one sample (n = 7,460). Rows and columns are clustered using Jensen-Shannon distance, and the heatmap is colored by row z-score. Each heatmap column represents the mean expression across three biological replicates for a sample. Sample labels are structured as follows: <experiment stage>_<time since stimulation>_<polarization condition>_<repolarization condition>. Experiment stage is either "Pol" (first 24h of polarization) or "RP" (subsequent 72h after media switch). Time since stimulation refers to hours since the last cytokine stimulation (either initial polarization or media switch). Polarization condition describes the cytokine treatment for the first 24h of polarization, (*legend continued on next page*)

Figure 2.10: (*continued*) while repolarization condition (where applicable) describes the cytokine treatment after the media switch. The color coding categorizes samples by the overall polarization/repolarization trajectory.

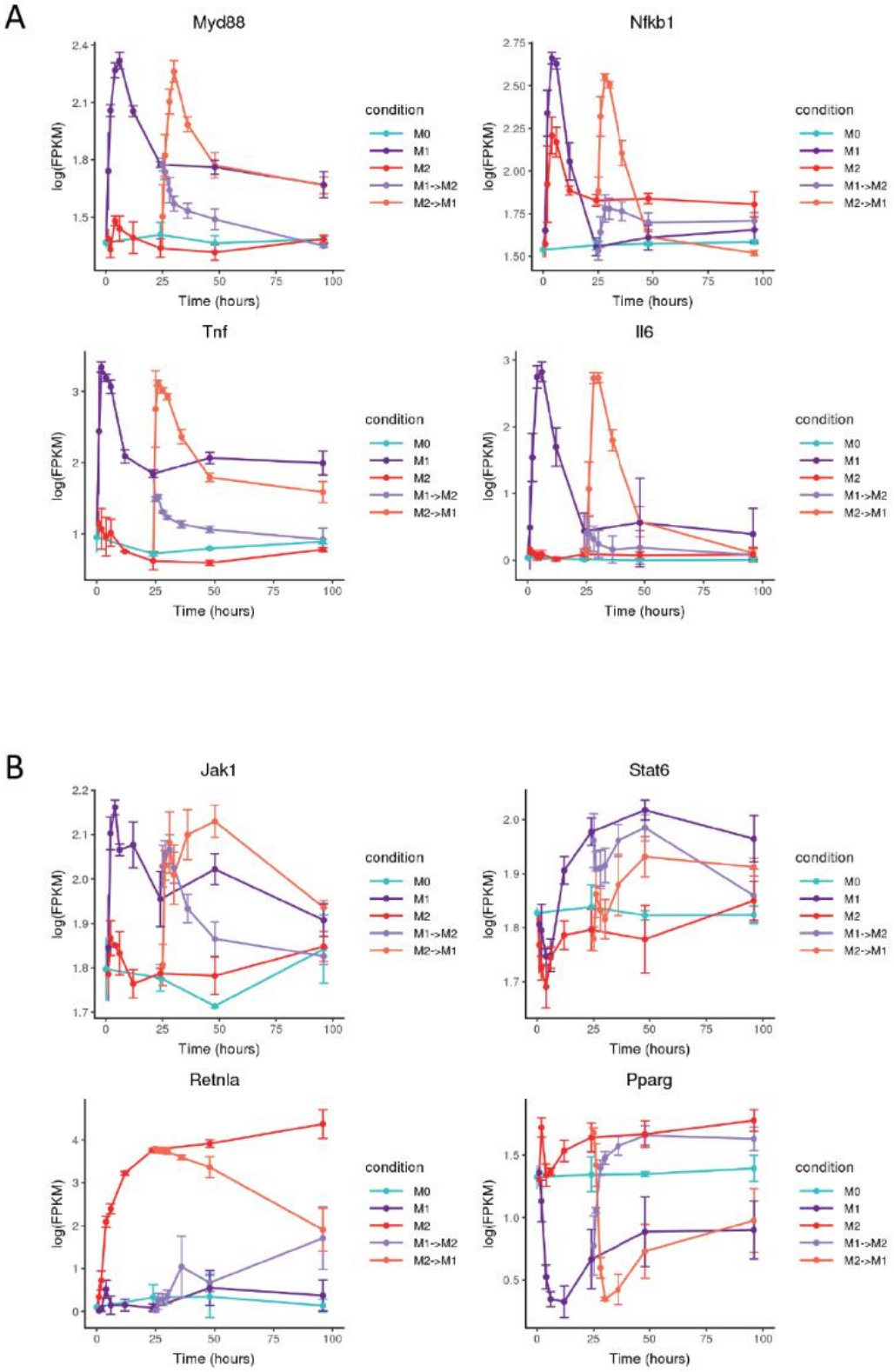

Figure 2.11: Gene expression of key M1 and M2 marker genes during polarization and repolarization.
(*legend continued on next page*)

Figure 2.11: (*continued*) A) Plots of the expression of M1 marker genes over time during macrophage polarization and subsequent repolarization (n = 3). B) Plots of the expression of M2 marker genes over time during macrophage polarization and subsequent repolarization (n = 3). Some genes, such as *Nfkb1* and *Jak1*, are active in both M1 and M2 polarization, leading to some overlap in expression patterns.

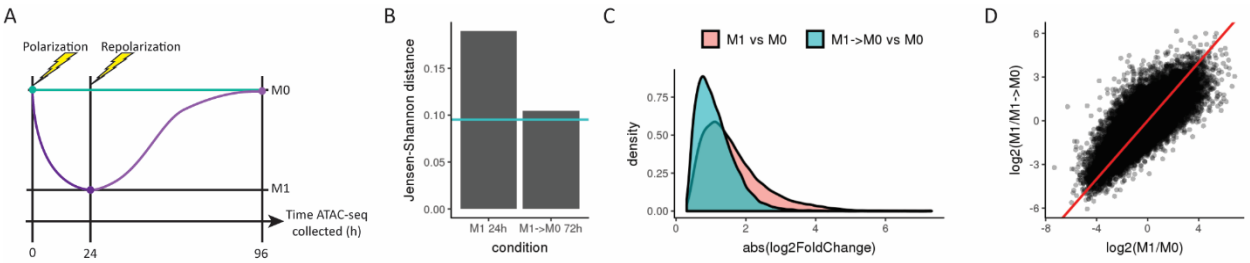

Figure 2.12: Macrophage chromatin accessibility also reverts to a baseline state when polarizing cytokines are removed.

A) Schematic of experimental design, where each point represents a collected sample, and each colored trajectory represents a different treatment condition. Murine bone marrow-derived macrophages were treated with IFN-γ + LPS to induce polarization to M1. After 24 hours, cells were washed to remove cytokines and then cultured in base media with no polarizing cytokines for an additional 72 hours (n = 3). B) Bar plot depicts Jensen-Shannon distance (JSD) between the ATAC accessibility profiles of polarized and depolarized macrophages compared to the 0h M0 control. As a baseline for expected global expression differences between samples, the teal line shows the average inter-replicate JSD between the three replicates for the 0h M0 control sample. JSD values for 24 M1 and 72h M1→M0 conditions were computed as the average of JSDs for all unique pairs between the three replicates of each treatment condition and the three replicates of the 0h M0 control. C) Density plots of log2 fold-change (absolute value) of chromatin accessibility for M1-polarized macrophages and M1→M0 depolarized macrophages compared to the baseline M0 condition. Median magnitude of log2 fold-change in chromatin accessibility is smaller for the M1→M0 depolarized macrophages compared to the M1-polarized macrophages. D) Scatterplot comparing log2 fold-change of chromatin accessibility for M1-polarized macrophages versus M0 (x-axis) and M1-polarized macrophages versus M1→M0 depolarized macrophages (y-axis). The red line (y = x) indicates the expected correlation in the case where M1→M0 depolarized macrophages are identical to M0 macrophages.

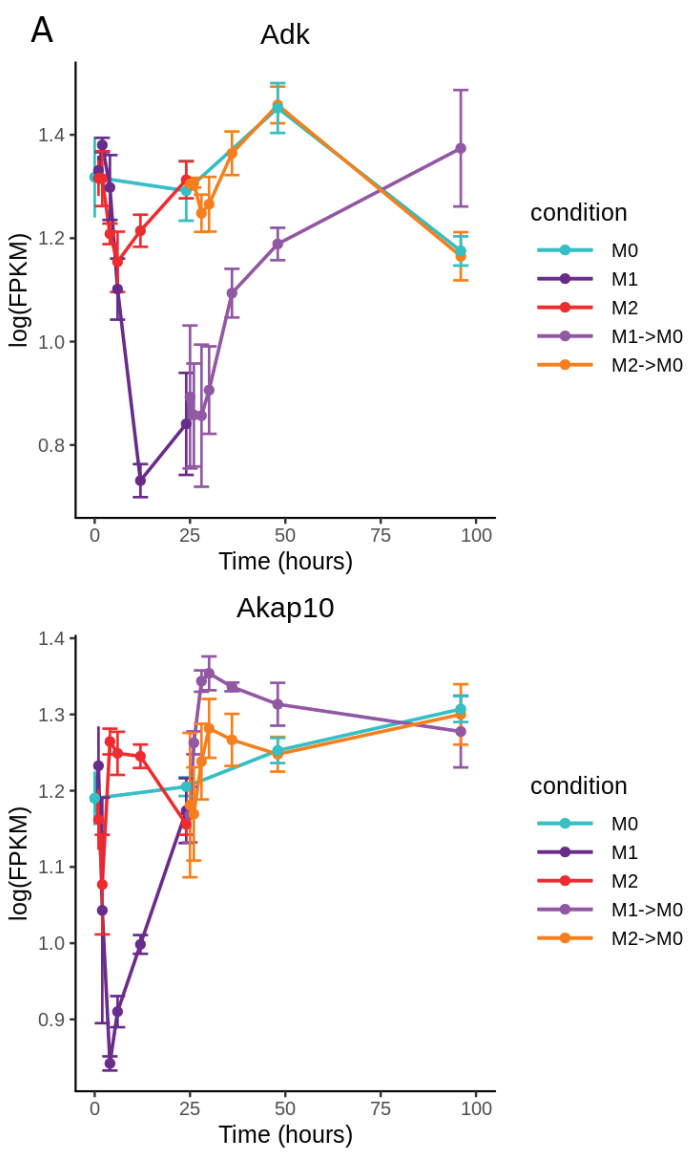

B

M1->M0 vs M0 (4-fold more accessible)
Gm38256
Akap10
Adk
Zfpm
2Spats2l
Gramd1c
Prkg1
Garnl3
Gm43302
Nr3c2

Figure 2.13: Differentially accessible genes between M1→M0 and M0.

Sites which were significantly more accessible in M1→M0 compared to M0 ($q < 0.05$) were further filtered to identify sites which were located within 500bp of a gene transcription start site and which exhibited at least a four-fold change in accessibility. A) Plots of gene expression vs. time for the genes which were linked to four-fold differentially accessible sites and also detected in the bulk RNA-seq timecourse data (n = 3). B) Full list of genes linked to sites which were four-fold more accessible in M1→M0 compared to M0. All 10 genes listed were also linked to sites which were four-fold more accessible in M1 compared to M0.

Chapter 3. DISSECTING ALVEOLAR MACROPHAGE FATE SPECIFICATION *IN VITRO*

In chapter 2, I describe my work characterizing the polarization and repolarization of bone-marrow derived macrophages *in vitro* between narrowly defined "M1" and "M2" states. In this well-defined cell culture context, macrophages exhibit an incredible degree of phenotypic plasticity: macrophage phenotype appears to depend solely on the stimuli present in the current microenvironment; upon exposure to new stimuli, macrophages will readily repolarize to a new state, and upon removal of external stimuli, macrophages will return to a baseline, unpolarized state. However, macrophages in the context of a living organism reside in much more complex microenvironments and are exposed to many different signals at once. While tissue-resident macrophages have also shown evidence of phenotypic plasticity (Lavin et al., 2014), it is not clear which signals in the tissue microenvironment are responsible for driving macrophage repolarization to the new tissue-specific phenotype. In this chapter, I describe some preliminary work dissecting the key stimuli responsible for determining alveolar macrophage fate.

3.1 INTRODUCTION

As tissue-resident macrophages of the lung, alveolar macrophages (AMs) are located along the distal epithelial surfaces of the lung. One key function of AMs is the clearance of pulmonary surfactant, a lipid-rich substance produced by alveolar epithelial type II cells that helps to reduce surface tension and prevent airspace collapse in the lung alveoli (Slovinsky et al., 2019). Granulocyte-macrophage colony stimulating factor (GM-CSF) plays a crucial role in AM regulation of surfactant homeostasis: knocking out the gene encoding the GM-CSF cytokine leads

to disruptions in downstream signaling pathways mediated by PU.1 and PPAR-γ that control the expression of several key lipid transporter genes, ultimately resulting in massive accumulation of lipids and phospholipids as AMs are unable to effectively clear surfactant (Ikegami et al., 1996; Yoshida et al., 2001; Berclaz et al., 2007; Baker et al., 2010). While AMs are responsible for clearing surfactant, substances contained in pulmonary surfactant have also been shown to play a role in regulating AM behavior (Fessler and Summer, 2016).

Lavin et al. (2014) previously demonstrated that peritoneal macrophages transferred into the lung subsequently adopted molecular profiles specific to alveolar macrophages, upregulating lung macrophage-specific genes and downregulating peritoneal macrophage-specific genes. Given macrophages' demonstrated phenotypic plasticity, we wished to explore what external stimuli would be sufficient to induce the AM phenotype in bone marrow-derived macrophages (BMDMs). Since surfactant metabolism is a key role of AMs, and since surfactant is prevalent within the lung microenvironment, we hypothesized that surfactant or one of its component substances might be a crucial signal for specifying AM fate.

To investigate this hypothesis, our collaborators at Cincinnati Children's Hospital cultured BMDMs *in vitro* and treated them with a combination of macrophage colony stimulating factor (M-CSF), granulocyte-macrophage colony stimulating factor (GM-CSF), and/or survanta, a synthetic surfactant substitute (see **Table 3.1** for a full list of conditions and **Figure 3.1** for a schematic of the experimental setup). We then profiled these macrophages using sci-RNAseq.

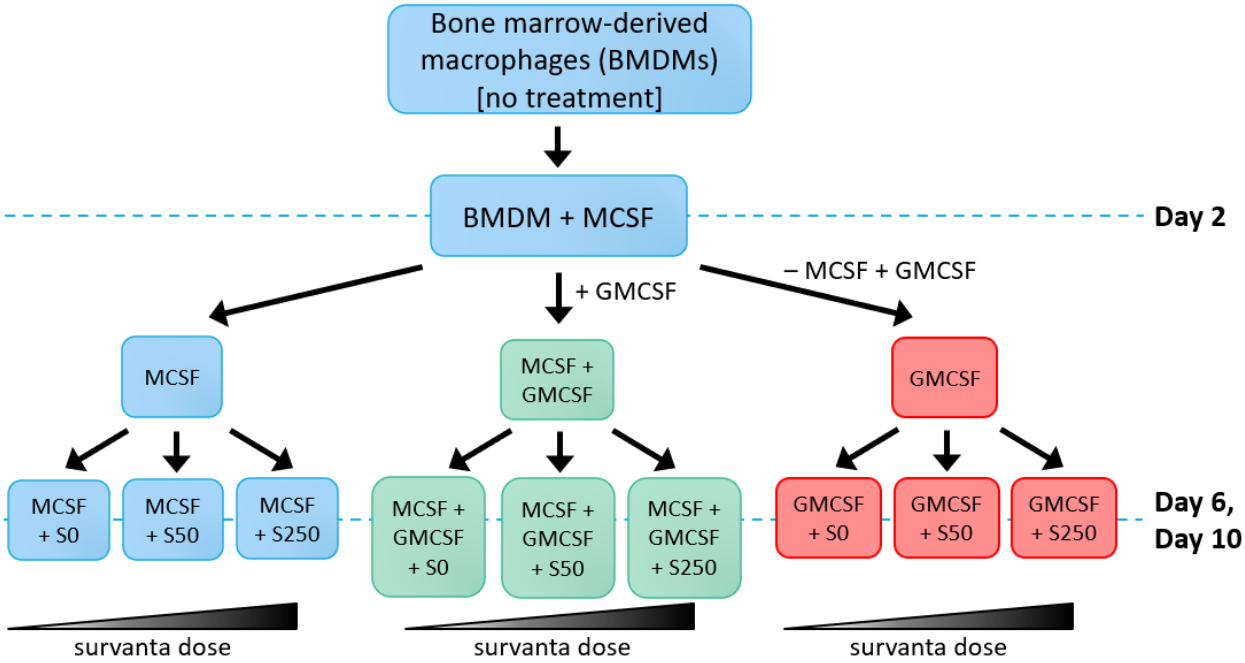

Figure 3.1: Experimental schematic for BMDM treatment with GM-CSF and survanta.

Murine bone marrow-derived macrophages (BMDMs) were treated with 10 ng/ml doses of either M-CSF, GM-CSF, or M-CSF+GM-CSF cytokines and survanta doses of 0 ug/ml, 50 ug/ml, or 250 ug/ml. Samples were collected at Day 2 (after initial cell plating) for the M-CSF-only baseline control, and at Days 6 and 10 for all treatment conditions, resulting in a total of 19 samples collected per biological replicate.

Table 3.1: Treatment conditions for *in vitro* BMDM samples.

Sample Name	Cytokine(s) [10 ng/ml dose each]	Survanta Dose (ug/ml)	Timepoint (days post-treatment)
MCSF 2d	MCSF	0	2
MCSF 6d	MCSF	0	6
GMCSF 6d	GMCSF	0	6
MCSF+GMCSF 6d	MCSF + GMCSF	0	6
MCSF+S50 6d	MCSF	50	6
GMCSF+S50 6d	GMCSF	50	6
MCSF+GMCSF+S50 6d	MCSF + GMCSF	50	6
MCSF+S250 6d	MCSF	250	6
GMCSF+S250 6d	GMCSF	250	6
MCSF+GMCSF+S250 6d	MCSF + GMCSF	250	6
MCSF 10d	MCSF	0	10
GMCSF 10d	GMCSF	0	10
MCSF+GMCSF 10d	MCSF + GMCSF	0	10
MCSF+S50 10d	MCSF	50	10
GMCSF+S50 10d	GMCSF	50	10
MCSF+GMCSF+S50 10d	MCSF + GMCSF	50	10
MCSF+S250 10d	MCSF	250	10
GMCSF+S250 10d	GMCSF	250	10
MCSF+GMCSF+S250 10d	MCSF + GMCSF	250	10

3.2 PRELIMINARY RESULTS

3.2.1 *Quality of sci-RNAseq data from BMDMs is not yet robust across experimental replicates*

Although our original experimental design included two *ex vivo* AM controls, meant to be processed in parallel with the BMDM samples as a benchmark of the alveolar macrophage phenotype, these plans proved infeasible due to our struggles with getting viable single-cell RNAseq data from AMs harvested via bronchoalveolar lavage, using either sci-RNAseq or 10X platforms (c.f. chapter section 5.1). Even sci-RNAseq on *in vitro* BMDMs proved to be less robust than we had hoped: while we were able to achieve UMI/cell recovery rates on the order of a few hundred UMIs/cell (UMI = “unique molecular identifier,” with each UMI corresponding to a unique mRNA transcript molecule) by using a combination of paraformaldehyde (PFA) fixation and either 2-level or 3-level sci-RNAseq, cell recovery rates varied widely by sample

and were quite low (n < 20) in several cases. Out of three total experimental replicates, the first processed using 2-level sci-RNAseq and the latter two processed using 3-level sci-RNAseq, only the second replicate yielded consistently robust recovery rates for both cells per sample and UMIs per cell (**Table 3.2**).

Table 3.2: Cell and UMI counts for BMDM samples.

Sample Name	Rep #1 [2-level sci]		Rep #2 [3-level sci]		Rep #3 [3-level sci]	
	# cells	Median UMIs/cell	# cells	Median UMIs/cell	# cells	Median UMIs/cell
MCSF 2d	14	134	72	184	27	147
MCSF 6d	133	216	745	287	143	132
GMCSF 6d	321	512	1004	318	376	136
MCSF+GMCSF 6d	537	684	1663	313	448	132
MCSF+S50 6d	216	244	926	291	225	133
GMCSF+S50 6d	190	490	681	347	261	139
MCSF+GMCSF+S50 6d	545	391	1943	368	913	140
MCSF+S250 6d	191	256	703	254	200	132
GMCSF+S250 6d	292	708	877	412	485	151
MCSF+GMCSF+S250 6d	547	507	1509	518	2082	164
MCSF 10d	479	317	1200	265	508	138
GMCSF 10d	73	220	233	318	6	138
MCSF+GMCSF 10d	54	180	561	373	16	116
MCSF+S50 10d	73	152	1093	313	668	152
GMCSF+S50 10d	2	113	514	390	12	116
MCSF+GMCSF+S50 10d	455	591	365	300	37	144
MCSF+S250 10d	297	1059	1337	328	731	161
GMCSF+S250 10d	217	302	684	328	76	136
MCSF+GMCSF+S250 10d	366	490	772	350	184	140

3.2.2 *GM-CSF treatment induces global transcriptomic changes but is insufficient to trigger AM specification*

Preliminary analysis of the second replicate reveals clear segregation between cells treated with a cytokine combination including GM-CSF (GM-CSF and GM-CSF+M-CSF conditions) and cells treated with only M-CSF (**Figure 3.2A**). However, there is no clear separation by survanta dose, or even by the presence or absence of survanta treatment (**Figure 3.2B**). Key downstream

signaling genes, such as PPAR-γ, also do not appear to be significantly differentially expressed based on cytokine treatment. These preliminary results suggest that although GM-CSF is required for AM function, it is not sufficient, either alone or in combination with survanta, to trigger activation of the AM program in BMDMs.

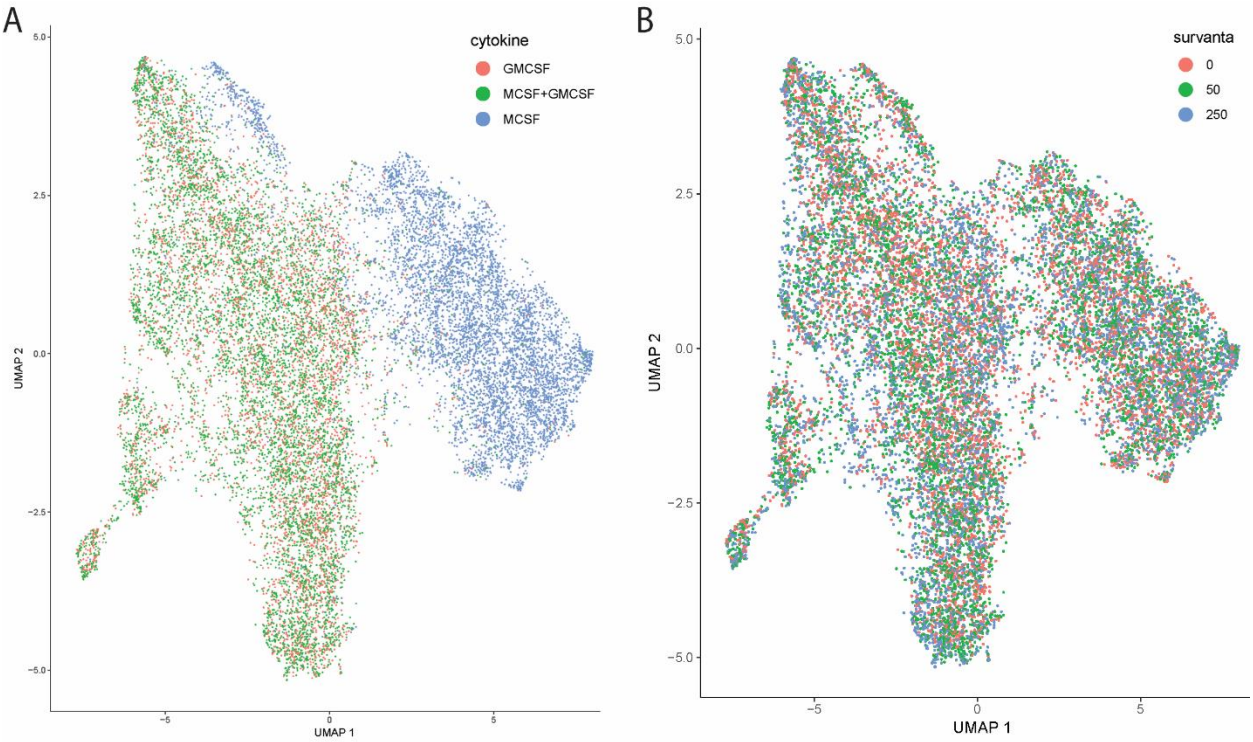

Figure 3.2: BMDMs segregate by cytokine treatment but not by survanta dose.

Murine bone marrow-derived macrophages (BMDMs) were treated with 10 ng/ml doses of either M-CSF, GM-CSF, or M-CSF+GM-CSF cytokines and survanta doses of 0 ug/ml, 50 ug/ml, or 250 ug/ml. Single-cell RNA-seq data was collected via 3-level sci-RNAseq for 16,882 cells and visualized after dimensionality reduction via UMAP, with individual cells colored by either A) cytokine treatment or B) survanta dose. Data shown here is from the second replicate listed in **Table 3.2**.

3.3 DISCUSSION

Single-cell combinatorial indexing RNA-sequencing (sci-RNAseq) has proved to be challenging in macrophages, and especially difficult in alveolar macrophages (AMs). Thus far,

we have failed to collect viable sci-RNAseq data from BAL-harvested AMs and have only been able to profile AMs by dissociating and fixing nuclei directly from frozen whole lung tissue (described further in section 5.1). While sci-RNAseq on bone marrow-derived macrophages (BMDMs) has been somewhat successful, data quality thus far has varied across replicates and is still not consistently robust.

BMDMs treated with either GM-CSF or a combination of GM-CSF and M-CSF cluster separately from cells treated with only M-CSF, suggesting that GM-CSF does induce global changes in gene expression (thus causing cells that receive GM-CSF to cluster separately from those that have not, since they will have similar overall gene expression patterns). However, GM-CSF does not appear to trigger upregulation of key downstream genes involved in lipid metabolism, such as PPAR-γ, indicating that GM-CSF alone is insufficient to induce the alveolar macrophage phenotype.

Treatment with survanta does not appear to cause any significant changes in global gene expression. One possible explanation is that survanta, a pharmaceutical cholesterol-free surfactant, is missing some key component normally found in pulmonary surfactant, which would trigger alveolar specification. Alternatively, multiple triggers in the alveolar microenvironment may normally be necessary to induce AM fate, and surfactant or survanta alone may be insufficient to trigger a transcriptomic response. Since PPAR-γ activation is a key component of AM fate specification, one potential follow-up experiment would be to screen multiple possible lipids or surfactant components to see which factors (or which combinations of factors) is able to induce PPAR-γ localization to the nucleus. Factors that passed this initial screen could then be tested to see whether they could induce alveolar specification in BMDMs, either alone or in combination with one another.

3.4 METHODS

3.4.1 *Macrophage cell culture*

Bone marrow-derived macrophages were harvested from wild-type C57BL/6J mice by our Cincinnati collaborators and cultured with 10 ng/ul M-CSF for 2 days (baseline condition). BMDMs were then treated with 10 ng/ml doses of either M-CSF, GM-CSF, or M-CSF+GM-CSF cytokines and survanta doses of 0 ug/ml, 50 ug/ml, or 250 ug/ml. BMDMs were harvested at 2 days for the baseline control, and 6 days and 10 days for the nine treatment conditions. Harvested macrophages were frozen and shipped to Seattle for single-cell RNA-sequencing.

3.4.2 *Library preparation*

Single cell RNA-seq libraries were generated according to the protocols described in Cao et al. (2017) for 2-level sci-RNAseq and Cao et al. (2019) for 3-level sci-RNAseq, with nuclei fixed in 5% paraformaldehyde. Libraries were sequenced on the Illumina NextSeq 500 platform using a v2 75-cycle kit (Read1: 18 cycles, Read 2: 52 cycles, Index 1: 10 cycles, Index 2: 10 cycles).

3.4.3 *Read alignments and construction of the expression matrices*

Base calls were converted to fastq format and demultiplexed using Illumina's bcl2fastq/2.16.0.10. Demultiplexed reads were aligned to the mouse reference genome (mm10) using STAR v2.5.2 with the following parameters: --runThreadN 20 --genomeLoad LoadAndKeep --outSAMstrandField intronMotif (Dobin et al., 2013). Expression matrices were generated by counting the number of unique UMIs per gene per cell.

3.4.4 *RNA-seq analysis*

The gene expression matrix was loaded into R (v3.6.1) (R Core Team, 2018) and analyzed using Monocle 3 (v0.2.0) (Qiu et al., 2017; Trapnell et al., 2014). To generate the UMAP plot, data normalization and preprocessing were run with the default parameter settings, dimensionality reduction and cell clustering were run using the UMAP reduction method option (Becht et al., 2018), and graph learning was run using learn_graph_control = list(ncenter=1000), and default settings otherwise. Figures were generated using ggplot2 (Wickham, 2009).

Chapter 4. MOLECULAR CHARACTERIZATION OF PULMONARY MACROPHAGE TRANSPLANTATION (PMT) THERAPY AT SINGLE-CELL RESOLUTION

4.1 INTRODUCTION

Suzuki et al. (2014) first introduced pulmonary macrophage transplantation (PMT) therapy, a treatment where wild type or GM-CSF gene-corrected macrophages are introduced into the lungs of GM-CSF deficient mice, which are used as a model of hereditary pulmonary alveolar proteinosis (hPAP). The transplanted wild type macrophages were able to take over normal alveolar macrophage (AM) functions like surfactant clearance, restoring proper lung function and rescuing the phenotype of the sick mice. The effects of the treatment were persistent long-term and were still evident even two years after the initial transplantation treatment.

The PMT system provides a framework where macrophages are undergoing dramatic phenotypic changes; the transplanted macrophages are adopting an alveolar phenotype in response to signals in the lung microenvironment and are also directly impacting their environment by clearing out excess surfactant to rescue the hPAP phenotype. Our goal is to characterize these changes on a molecular level by profiling macrophages in the lungs of PMT mice over the course of their treatment and recovery using single-cell RNA-seq and single-cell ATAC-seq.

4.2 PRELIMINARY RESULTS

4.2.1 *Whole-lung 2-level sci-RNAseq successfully captures single-cell transcriptomic data from alveolar macrophages*

Although performing sci-RNAseq on AMs harvested via bronchoalveolar lavage (BAL) has proved to be quite challenging, we have had more success with trying sci-RNAseq on whole lungs which are simultaneously fixed and dissociated into a single cell suspension (c.f. chapter section 5.1). Since we ultimately want to characterize macrophage development over the course of PMT treatment (on a timescale of months to years), we will need to be able to acquire high quality single-cell RNA-seq data from mouse lungs displaying hPAP symptoms to different degrees.

As a preliminary test, we first performed 2-level sci-RNAseq on lungs collected from both wild type (WT) and two different strains of GM-CSF deficient mice. In total, four different conditions were represented: 1) 6 week-old WT mice; 2) 6 week-old GM-KO (*Csf2* -/-) mice, in which the GM-CSF gene was knocked out; 3) 6 week-old GM-RbcKO (*Csf2rb* -/-) mice, in which the GM-CSF receptor gene was knocked out; and 4) 2 year-old WT mice (summarized in **Table 4.1**; schematic in **Figure 4.1**). Frozen mouse lungs were simultaneously fixed with 5% glutaraldehyde and physically dissociated using the Miltenyi Biotech gentleMACS, then repeatedly washed and filtered to generate a single nuclei suspension. Nuclei yield from individual lungs was quite high overall, numbering ~10 million on the low end and over 60 million on the high end. 2-level sci-RNAseq on the fixed nuclei resulted in good cell and mRNA yield, although surprisingly, the KO lungs performed substantially better than the WT lungs (**Table 4.2**). Normally, after accounting for inefficiencies and loss during library prep and sequencing, we expect to recover ~50% of the cells that are sorted during the FACS step in 2-

level sci-RNAseq. Since 960 cells were sorted for each sample in the experiment, this amounts to an expected cell yield of ~480 cells per sample. By this benchmark, cell yield for the both WT samples is on the low side, while cell yield for the KO lungs is extraordinarily high, outperforming our expectations (~800/960 = ~83% cell yield).

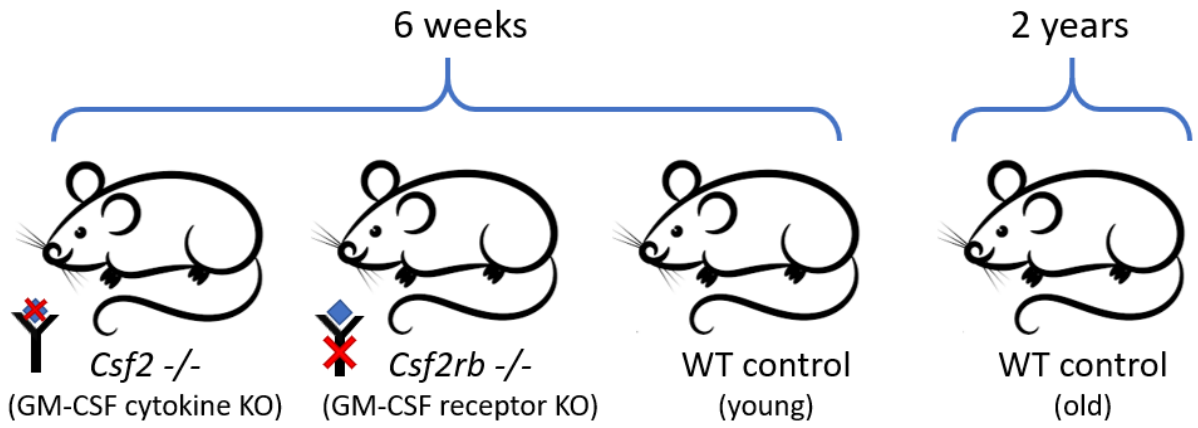

Figure 4.1: Schematic of mouse conditions for preliminary whole lung sci-RNAseq.

Four mouse conditions are represented in total. The two knockout conditions represent two different models of pulmonary alveolar proteinosis: in one strain, the gene for the GM-CSF cytokine is knocked out (*Csf2 -/-*), while in the other strain, the gene for the GM-CSF receptor is knocked out (*Csf2rb -/-*). The two wild type conditions consist of a 6-week old control which is age-matched to the two knockout mice conditions and a 2-year old control which represents the expected age of mice at the end of PMT treatment.

Table 4.1: List of mouse strains for preliminary whole lung sci-RNAseq.

Sample Name	Strain	Age	Description
WT_young	Wild type	6 weeks	Young wild type mice (age-matched to KO strains)
GM_KO	*Csf2 -/-*	6 weeks	Knockout of the GM-CSF gene
GM_RbcKO	*Csf2rb -/-*	6 weeks	Knockout of the GM-CSF receptor gene
WT_old	Wild type	2 years	Old wild type mice (simulating treatment end point)

Table 4.2: Cell and UMI counts for whole lung sci-RNAseq samples.

Sample Name	Rep #1 [2-level sci]		Rep #2 [3-level sci]		Rep #3 [3-level sci]	
	# cells	Median UMIs/cell	# cells	Median UMIs/cell	# cells	Median UMIs/cell
WT_young	180	477	102	134	29	112
GM_KO	804	1118	3670	168	2041	166
GM_RbcKO	846	2018	4163	202	5149	197
WT_old	339	509	478	138	357	133

Visualizing the sci-RNAseq data in a reduced dimensionality space reveals several well-defined cell clusters, which appear to correlate to canonical lung cell types (e.g. alveolar type I and type II cells), including macrophages (**Figure 4.2**). However, cells identified as macrophages (n = 34) comprise only a small portion (~1.6%) of the total cell population (n = 2169), and we will likely need to profile a larger number of macrophages per lung in order to capture the effects of PMT over the course of treatment. This suggests that we may need to either scale up the scope of our sci-RNAseq experiments (i.e. collect data for a large enough number of lung cells, such that even a small percentage of the total will still amount to a sizeable macrophage sample size) or implement some kind of selection to preferentially capture macrophages from the population of all lung cells.

4.2.2 *Whole-lung 3-level sci-RNAseq yields inconsistent results and fails to capture data for WT lungs*

Because 3-level sci-RNAseq uses an additional level of indexing, it has the potential to accommodate much higher experimental throughput compared to 2-level sci-RNAseq (Cao et al., 2019). To test the feasibility of 3-level sci-RNAseq in conjunction with our whole lung pre-processing workflow, we processed two additional sets of frozen mouse lungs in the same manner

as the first replicate (simultaneous fixation in 5% glutaraldehyde and physical dissociation via gentleMACS, followed by washes and filtering to produce a single nuclei suspension). We then submitted aliquots of each sample to the Brotman Baty Institute (BBI) for 3-level sci-RNAseq processing.

However, our results from 3-level whole lung sci-RNAseq were somewhat mixed: while we did indeed recover a larger number of cells for the two KO mouse strains, we recovered much fewer cells for the WT samples (**Figure 4.3**). In the case of the 6 week-old WT lungs, cell recovery from 3-level sci-RNAseq was substantially worse than from 2-level sci-RNAseq, with only 27 cells for the third replicate. Additionally, UMI/cell recovery was uniformly worse for 3-level sci-RNAseq compared to 2-level sci-RNAseq (**Table 4.2**). Consequently, further optimization would be necessary to ensure robust cell recovery across all sample types and to increase UMI yield before 3-level sci-RNAseq could be used for large-scale processing of whole lung samples.

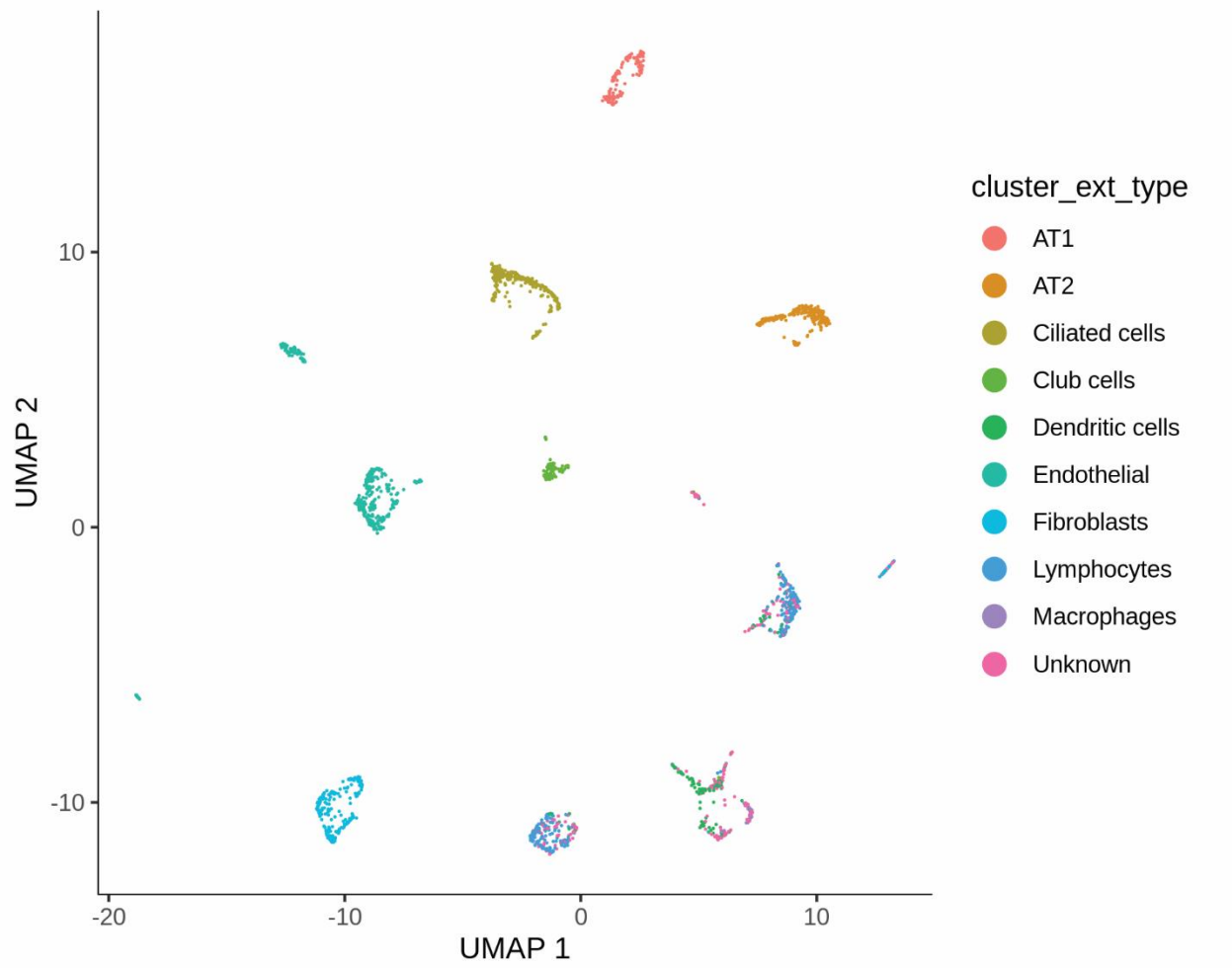

Figure 4.2: Whole lung sci-RNAseq captures canonical lung cell types.

Flash-frozen whole mouse lungs were fixed in glutaraldehyde and physically dissociated into a single nuclei suspension. Single-cell RNA-seq data was collected via 2-level sci-RNAseq for 2,169 cells and visualized after dimensionality reduction via UMAP. Cell type was determined by using a marker-free Garnett classifier trained on a previously annotated single-cell RNA-seq lung dataset (Franks, unpublished). Cells in the UMAP plot above are colored by their "cluster-extended cell type," which refers to the Garnett cell type assignment paradigm which uses cell cluster position to help determine cell types for initially "unknown" cells (e.g. an indeterminate cell located near many neighbors of a single known cell type may be assigned that cell type as its "cluster-extended cell type").

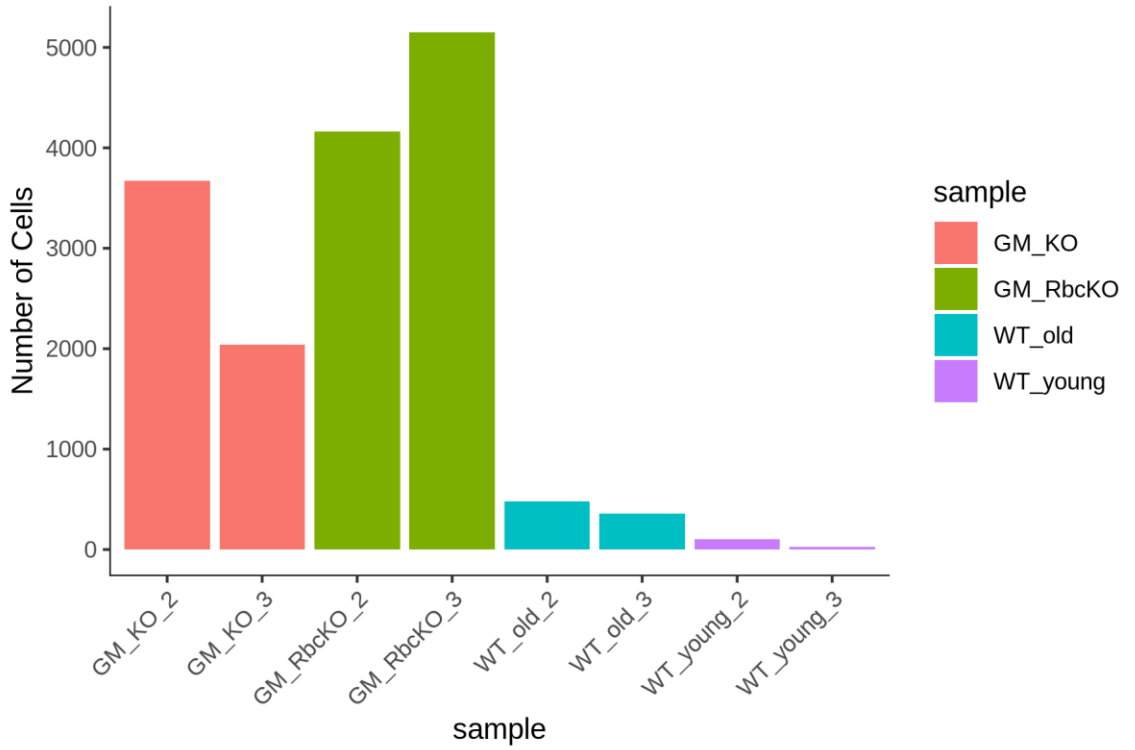

Figure 4.3: Whole lung 3-level sci-RNAseq captures KO cells but not WT cells.

Barplot of the number of cells captured (UMIs/cell ≥ 100); the number after each sample name indicates the biological replicate. While several thousand cells were captured for each of the knockout mouse lungs, very few cells were captured for any of the wild type mouse lungs.

4.3 Discussion

Our preliminary results from attempting 2-level and 3-level sci-RNAseq on mouse lungs show some promise, but further optimization will still be required before our current sample workflow would be suitable to scale up for a full PMT timecourse experiment. While 2-level sci-RNAseq on cells fixed and dissociated from frozen whole mouse lung tissue was able to recover single-cell resolution transcriptomic data from several canonical lung cell types, including the alveolar macrophages of interest, the overall proportion of macrophages within the total population of profiled cells was quite low (~1.6%). One possible solution for increasing the number of macrophages profiled is to use a higher throughput protocol, such as 3-level sci-RNAseq.

However, our 3-level sci-RNAseq single-cell data were of lower quality compared to the 2-level results, with lower overall UMI/cell capture rates across the samples and with very low cell recovery rates for the WT lung samples. Consequently, our 3-level sci-RNAseq sample workflow still requires optimization to improve both UMI/cell recovery and cell recovery rates.

One other bottleneck for scaling up whole lung sci-RNAseq is the sample pre-processing step. Under the current protocol, up to two lungs can be processed at once, and two sets of lungs (of up to two lungs per set) could be processed in a typical work day. Once processed, the suspensions of single, fixed nuclei can be flash-frozen and stored long-term in cryostorage, so as to be used for sci-RNAseq or other assays at a later date. Thus, the pre-processing step of converting whole lung tissue to fixed, frozen nuclei poses a serious bottleneck in the sample processing workflow, since only four lungs can be processed in a given day. The small sample throughput also introduces the possibility of batch effects, since only two lungs are processed simultaneously at any given time. Both of these limitations would be especially impactful as we attempt to scale up the experiment to profile macrophage development over the course of PMT treatment; even sampling a timecourse on the order of a timepoint every 2-3 months, continuing this over the 2-year course of treatment could easily yield over 20 samples for a single experimental replicate. Consequently, we would need to carefully consider the design of both the overall experiment and the allocation of samples for pre-processing in order to minimize the impact of batch effects on the final data.

4.4 METHODS

4.4.1 *Sample collection*

Whole lungs were harvested from 12 week-old wild-type, *Csf2 -/-*, and *Csf2rb -/-* mice, and from 2 year-old wild-type mice. Harvested lung tissue samples were frozen and shipped to Seattle for single-cell RNA-sequencing.

4.4.2 *Library preparation*

Frozen whole lungs were transferred directly into fixation/lysis buffer (10 mM sodium phosphate, 10 mM NaCl, 3 mM MgCl2, 10 mM vanadyl ribonucleoside complex, 1.9 uM polyvinyl sulfonate, 1% DEPC, 5% glutaraldehyde, 0.02% Triton X-100) and physically dissociated into a single nuclei suspension using the Miltenyi Biotech gentleMACS. Single-cell RNA-seq libraries were then generated according to the protocols described in Cao et al. (2017) for 2-level sci-RNAseq and Cao et al. (2019) for 3-level sci-RNAseq. Libraries were sequenced on the Illumina NextSeq 500 platform using a v2 75-cycle kit (Read1: 18 cycles, Read 2: 52 cycles, Index 1: 10 cycles, Index 2: 10 cycles).

4.4.3 *Read alignments and construction of the expression matrices*

Base calls were converted to fastq format and demultiplexed using Illumina's bcl2fastq/2.16.0.10. Demultiplexed reads were aligned to the mouse reference genome (mm10) using STAR v2.5.2 with the following parameters: --runThreadN 20 --genomeLoad LoadAndKeep --outSAMstrandField intronMotif (Dobin et al., 2013). Expression matrices were generated by counting the number of unique UMIs per gene per cell.

4.4.4 *RNA-seq analysis*

The gene expression matrix was loaded into R (v3.6.1) (R Core Team, 2018) and analyzed using Monocle 3 (v0.2.0) (Qiu et al., 2017; Trapnell et al., 2014). To generate the UMAP plot, data normalization and preprocessing were run with the default parameter settings, dimensionality reduction and cell clustering were run using the UMAP reduction method option (Becht et al., 2018), and graph learning was run using learn_graph_control = list(ncenter=1000), and default settings otherwise. Figures were generated using ggplot2 (Wickham, 2009).

Chapter 5. CLOSING REMARKS

In this dissertation, I describe my efforts to characterize macrophage polarization and repolarization using global transcriptomic profiling. I demonstrate that bone marrow-derived macrophages (BMDMs) exhibit a high level of phenotypic plasticity and adopt transient polarized phenotypes corresponding to stimuli in their immediate environment *in vitro*. I also describe preliminary work aimed at identifying key stimuli responsible for specifying alveolar macrophage fate and performing single-cell transcriptomic profiling of alveolar macrophages in the context of pulmonary macrophage transplantation therapy. In this final chapter, I discuss challenges and potential approaches for extending sci-RNAseq to primary tissue cells, and I summarize the main conclusions from my dissertation research.

5.1 Optimization of sci-RNAseq for primary tissue cells

While *in vitro* culture offers a flexible and easily accessible model for studying macrophage polarization, many interesting questions, such as profiling tissue-resident macrophage populations, rely on collecting data directly from primary tissue cells. In particular, I was collaborating with Dr. Bruce Trapnell (Cincinnati Children's Hospital) and his lab on projects aimed at characterizing murine alveolar macrophages in healthy and disease model settings using single-cell genomics. These experiments first necessitated that I establish a single-cell RNA-seq protocol that worked robustly on *ex vivo* alveolar macrophages, which are the tissue-resident macrophages specific to the lung. The scope of the planned experiments (many conditions x many timepoints) led us to favor the sci-RNAseq platform over 10X due to its flexibility and high potential throughput. However, applying sci-RNAseq to alveolar macrophages (AMs), and even to bone marrow-

derived macrophages (BMDMs), proved to be much more challenging than we had initially anticipated.

Our first attempts used 2-level sci-RNAseq (Cao et al., 2017) on mouse AMs which our Cincinnati collaborators had isolated via whole lung bronchoalveolar lavage (BAL), then frozen and shipped to us. When processed alongside mouse BMDMs, the AM samples exhibited significantly decreased cell recovery; while we recovered on the order of ~100 cells for each of 15 BMDM samples, one of the two AM samples dropped out entirely, while the other yielded only 12 cells. In the original 2-level sci-RNAseq protocol, pre-processing of cells or nuclei prior to reverse transcription involves fixation with methanol followed by a series of five washes. Since a fraction of the original input cells are lost after each wash, and since one of our main concerns was sample dropout due to low cell recovery, we first tried reducing the number of post-fixation washes. However, we found that while reducing the number of washes from the original five to one or two prevented sample dropout, this level of cell washing was insufficient to remove the residual methanol from fixation, and we were subsequently unable to recover mRNA from the washed cells. Further experimentation tweaking the wash volume (in an effort to dilute out methanol faster, even with fewer washes), wash spin speed, wash spin duration, spin tube (falcon vs. Eppendorf), and base buffer (phosphate-buffered saline vs. sodium citrate) produced some marginal improvements, but we were unable to find a set of conditions that yielded a viable level of both cell recovery per sample and UMI recovery per cell.

One fundamental challenge posed by working with BAL-harvested AMs is the limited cell input available per sample. A typical BAL sample contained ~100,000 cells, which is already on the low end for sci-RNAseq, even before factoring in subsequent losses from sample freeze-thaw. The limited input reduces the margin for error, but also makes certain protocol steps more difficult

and more prone to human error; for example, cell washes are more difficult to perform precisely when there are insufficient cells to form a visible pellet. Another challenge we faced in working with AMs is that several classes of endogenous RNases are particularly abundant in the lung (Lu et al., 2018). A high level of endogenous RNase likely contributed to our low UMI/cell recovery from AMs, since any residual uninhibited RNases could degrade cellular mRNA molecules before they can be reverse transcribed. These factors make it difficult to collect single-cell RNAseq data from BAL-harvested macrophages even on the 10X platform, which requires less sample preprocessing and is normally more robust than sci-RNAseq in terms of UMI/cell recovery. When we processed a BAL-harvested AM sample alongside a sample of peripheral blood mononuclear cells (PBMCs) using 10X, the cell yield for the AMs was almost 10-fold less than that for the PBMCs (~200 AMs vs. ~16,000 PBMCs). Additionally, many of the recovered AMs had a very high percentage of mitochondrial mRNA reads (over 50%), suggesting that these cells may have been damaged or otherwise depleted of nuclear and cytosomal mRNA. As a result, neither sci-RNAseq nor 10X could be considered reliable platforms for collecting single-cell RNAseq data from BAL-harvested AMs, and we turned instead to alternative approaches.

One of my colleagues in the Trapnell Lab, David Read, was also troubleshooting sci-RNAseq on primary tissue samples (lung and kidney), and had found some success in performing sci-RNAseq on whole tissue samples which were simultaneously fixed using glutaraldehyde and physically dissociated. Glutaraldehyde is a powerful protein crosslinker (Kiernan, 2000), and by simultaneously fixing and dissociating the tissues, cell exposure to active endogenous RNases can be minimized. When I tried using David's pre-processing protocol on flash-frozen mouse lungs followed by the usual 2-level sci-RNAseq workflow, I was able to collect high quality single-cell RNA-seq data, with good recovery for both cells per sample and UMIs per cell (preliminary results

described further in section 3.4.1). Adopting this approach offered several benefits: firstly, it streamlined the sample collection process for our Cincinnati collaborators, since the whole mouse lungs could simply be dissected, frozen, then shipped directly. Secondly, working with whole lungs neatly sidestepped the issue of low cell input per sample, since each mouse lung yields tens of millions of cells once dissociated. Finally, because this approach minimizes the amount of sample handling between tissue harvest and fixation, the data we collect is arguably a more faithful representation of the true transcriptomic landscape of the lung, since cells are not subjected to the stresses of BAL before being profiled. Hence, although some challenges still remain, particularly with regard to scaling up experiments, whole lung sci-RNAseq is a promising strategy for single-cell transcriptomic profiling of *ex vivo* alveolar macrophages.

5.2 Conclusions and future directions

Throughout the course of my dissertation research, I have investigated mechanisms of macrophage phenotypic plasticity in both *in vitro* and *ex vivo* contexts. In my work characterizing macrophage polarization and repolarization between canonical M1 and M2 states *in vitro*, I built upon previous research by Stout et al. (2004, 2005) showing that sequentially treating macrophages with different cytokines resulted in progression through multiple functional phenotypes. Stout et al. characterized cytokine-treated macrophages using ELISA and immunoblotting and found that changing cytokine treatments caused macrophages to alter the set of cytokine proteins that they secreted. By using bulk RNA-sequencing to profile macrophages that were sequentially treated with different cytokines *in vitro*, I measured global gene expression patterns for macrophages undergoing polarization and repolarization and was able to provide a broader view of the changes occurring in macrophage phenotype. By collecting fine-

scale timecourse data, I also elucidated the transcriptomic trajectories that macrophages followed over the course of polarization and established that macrophage phenotypes are highly transient, with little to no memory retained from past states.

Within the well-defined *in vitro* context of canonical M1/M2 macrophage states, my research strongly suggests that macrophages are extremely plastic and adopt transient phenotypes that correspond to their immediate microenvironment. However, macrophages in an *in vivo* context are subject to much more complex environments, and the phenotypic transience that I observed in cell culture may not hold in a tissue environment. Lavin et al. (2014) previously showed that tissue-resident macrophages still demonstrate phenotypic plasticity in that macrophages harvested from one tissue and then transplanted into a new tissue change to take on traits defined by the new tissue microenvironment. In an effort to better understand the mechanisms governing fate specification and function of tissue-resident macrophages, I embarked upon two projects aimed at characterizing alveolar macrophages, the tissue-resident macrophages of the lung.

In the first of these projects, I sought to identify some of the key stimuli within the lung environment that were responsible for inducing alveolar macrophage fate. By culturing bone marrow-derived macrophages *in vitro* with different combinations of cytokines and lipid stimuli, I was able to characterize the impact of specific stimuli on macrophage phenotype either in isolation or in controlled combinations. Preliminary results from these experiments suggested that while granulocyte colony macrophage stimulating factor (GM-CSF) induces changes in global gene expression patterns, it is not sufficient to turn on key downstream alveolar signaling pathways, such as PPAR-γ. Furthermore, treatment with survanta, a pharmaceutical surfactant, does not appear to significantly impact macrophage gene expression profiles. While my work has

begun to characterize two possible stimuli involved in alveolar macrophage development, there are many other potential stimuli in the lung microenvironment. Single-cell RNA-sequencing provides a high-resolution, global snapshot of macrophage states, but can also be costly to perform. Therefore, a first step for future work towards dissecting the drivers of alveolar macrophage fate may be to perform a GFP-based functional screen to determine which stimuli (or combinations of stimuli) are able to induce PPAR-γ localization to the nucleus in bone marrow-derived macrophages. This would identify a shortlist of candidates that could then be assayed using single-cell RNA-sequencing.

My second project aimed to profile alveolar macrophages in the context of pulmonary macrophage transplantation (PMT) therapy, which is a potential treatment for pulmonary alveolar proteinosis (PAP). In PAP, alveolar macrophages do not mature properly and are unable to perform their normal functions, including surfactant clearance; PMT introduces into the lung functional macrophages that are able to take over normal alveolar macrophage roles, thus restoring a healthy phenotype. Single-cell RNA-seq profiling of macrophages over the course of PMT could potentially give insight into how transplanted macrophages are able to adopt alveolar macrophage traits and functions. One traditional method of collecting alveolar macrophages for characterization is to perform bronchoalveolar lavage (BAL) and then isolate alveolar macrophages from the BAL fluid. However, in my exploratory work for this project, I quickly discovered that neither 10X nor single-cell combinatorial indexing RNA-sequencing (sci-RNAseq) protocols could consistently capture high quality single-cell RNA-seq data from BAL-harvested macrophages. Subsequent efforts at performing sci-RNAseq on whole lung tissue, rather than on BAL-harvested macrophages, have shown some preliminary success, but are not yet robust across sample types and across replicates. In particular, 3-level sci-RNAseq suffers in

terms of cell yield and UMIs/cell, especially for lungs collected from wild-type mice. One possible reason that 3-level sci-RNAseq may perform worse than 2-level sci-RNAseq is that cells are separated into PCR wells by dilution instead of by fluorescence activated cell sorting (FACS). Since flow sorting helps to filter out debris that might otherwise contaminate downstream reactions, adding a sorting step back into the 3-level sci-RNAseq workflow could be a first step in future work to continue optimizing sci-RNAseq protocols for primary lung cells.

Overall, my research suggests that macrophages are particularly mutable, readily adapting in response to new stimuli or new microenvironments. In an *in vitro* context, M1- and M2-polarized macrophages are more akin to transient phenotypic states rather than canonical "cell types," with macrophages readily changing phenotypes to match their current environment. Tissue microenvironments *in vivo* present a much more complex context, and while tissue-resident macrophages have still been shown to be phenotypically malleable, the specific stimuli triggering such changes are not well characterized. Single-cell RNA-sequencing is a powerful tool for dissecting these complex environments; once properly optimized to yield robust results on primary cells, these technologies will enable researchers to study macrophage plasticity *in vivo* at high resolution, opening up a spectrum of new avenues for discovery.

BIBLIOGRAPHY

Abraham, D., Zins, K., Sioud, M., and Lucas, T. (2010). Stromal cell-derived CSF-1 blockade prolongs xenograft survival of CSF-1-negative neuroblastoma. J. Cancer. *126*, 1339-52.

Aharinejad, S., Sioud, M., Lucas, T., and Abraham, D. (2009). Targeting stromal-cancer cell interactions with siRNAs. Methods Mol. Biol. *487*, 243–266.

Andreu, P., Johansson, M., Affara, N.I., Pucci, F., Tan, T., Junankar, S., Korets, L., Lam, J., Tawfik, D., DeNardo, D.G., et al. (2010). FcRγ Activation Regulates Inflammation-Associated Squamous Carcinogenesis. Cancer Cell *17*, 121–134.

Baker, A.D., Malur, A., Barna, B.P., Kavuru, M.S., Malur, A.G., and Thomassen, M.J. (2010). PPARgamma regulates the expression of cholesterol metabolism genes in alveolar macrophages. Biochem. Biophys. Res. Commun. *393*, 682–687.

Becht, E., McInnes, L., Healy, J., Dutertre, C.-A., Kwok, I.W.H., Ng, L.G., Ginhoux, F., and Newell, E.W. (2019). Dimensionality reduction for visualizing single-cell data using UMAP. Nat. Biotechnol. *37*, 38-44.

Bendall, S.C., Davis, K.L., Amir, E.-A.D., Tadmor, M.D., Simonds, E.F., Chen, T.J., Shenfeld, D.K., Nolan, G.P., and Pe'er, D. (2014). Single-cell trajectory detection uncovers progression and regulatory coordination in human B cell development. Cell *157*, 714–725.

Berclaz, P.-Y., Carey, B., Fillipi, M.-D., Wernke-Dollries, K., Geraci, N., Cush, S., Richardson, T., Kitzmiller, J., O'connor, M., Hermoyian, C., et al. (2007). GM-CSF regulates a PU.1-dependent transcriptional program determining the pulmonary response to LPS. Am. J. Respir. Cell Mol. Biol. *36*, 114–121.

Biswas, S.K., and Mantovani, A. (2010). Macrophage plasticity and interaction with lymphocyte subsets: cancer as a paradigm. Nat. Immunol. *11*, 889–896.

Buenrostro, J.D., Wu, B., Chang, H.Y., and Greenleaf, W.J. (2015). ATAC-seq: A Method for Assaying Chromatin Accessibility Genome-Wide. Curr. Protoc. Mol. Biol. *109*, 21.29.1–9.

Buscher, K., Ehinger, E., Gupta, P., Pramod, A.B., Wolf, D., Tweet, G., Pan, C., Mills, C.D., Lusis, A.J., and Ley, K. (2017). Natural variation of macrophage activation as disease-relevant phenotype predictive of inflammation and cancer survival. Nat. Commun. *8*, 16041.

Cao, J., Packer, J.S., Ramani, V., Cusanovich, D.A., Huynh, C., Daza, R., Qiu, X., Lee, C., Furlan, S.N., Steemers, F.J., et al. (2017). Comprehensive single-cell transcriptional profiling of a multicellular organism. Science *357*, 661–667.

Cao, J., Spielmann, M., Qiu, X., Huang, X., Ibrahim, D.M., Hill, A.J., Zhang, F., Mundlos, S., Christiansen, L., Steemers, F.J., et al. (2019). The single-cell transcriptional landscape of mammalian organogenesis. Nature *566*, 496–502.

Davies, L.C., Jenkins, S.J., Allen, J.E., and Taylor, P.R. (2013). Tissue-resident macrophages. Nat. Immunol. *14*, 986–995.

DeNardo, D.G., Barreto, J.B., Andreu, P., Vasquez, L., Tawfik, D., Kolhatkar, N., and Coussens, L.M. (2009). CD4+ T Cells Regulate Pulmonary Metastasis of Mammary Carcinomas by Enhancing Protumor Properties of Macrophages. Cancer Cell *16*, 91–102.

DeNardo, D.G., Andreu, P., and Coussens, L.M. (2010). Interactions between lymphocytes and myeloid cells regulate pro- versus anti-tumor immunity. Cancer Metastasis Rev. *29*, 309–316.

Dobin, A., Davis, C.A., Schlesinger, F., Drenkow, J., Zaleski, C., Jha, S., Batut, P., Chaisson, M., and Gingeras, T.R. (2013). STAR: ultrafast universal RNA-seq aligner. Bioinformatics *29*, 15–21.

Duluc, D., Corvaisier, M., Blanchard, S., Catala, L., Descamps, P., Gamelin, E., Ponsoda, S., Delneste, Y., Hebbar, M., and Jeannin, P. (2009). Interferon-gamma reverses the immunosuppressive and protumoral properties and prevents the generation of human tumor-associated macrophages. Int. J. Cancer *125*, 367–373.

DuPage, M., and Bluestone, J.A. (2016). Harnessing the plasticity of CD4(+) T cells to treat immune-mediated disease. Nat. Rev. Immunol. *16*, 149–163.

Epelman, S., Lavine, K.J., and Randolph, G.J. (2014a). Origin and functions of tissue macrophages. Immunity *41*, 21–35.

Epelman, S., Lavine, K.J., Beaudin, A.E., Sojka, D.K., Carrero, J.A., Calderon, B., Brija, T., Gautier, E.L., Ivanov, S., Satpathy, A.T., et al. (2014b). Embryonic and adult-derived resident cardiac macrophages are maintained through distinct mechanisms at steady state and during inflammation. Immunity *40*, 91–104.

Fessler, M.B., and Summer, R.S. (2016). Surfactant Lipids at the Host-Environment Interface. Metabolic Sensors, Suppressors, and Effectors of Inflammatory Lung Disease. Am. J. Respir. Cell Mol. Biol. *54*, 624–635.

Goerdt, S., Politz, O., Schledzewski, K., Birk, R., Gratchev, A., Guillot, P., Hakiy, N., Klemke, C.D., Dippel, E., Kodelja, V., et al. (1999). Alternative versus classical activation of macrophages. Pathobiology *67*, 222–226.

Gordon, S. (2003). Alternative activation of macrophages. Nat. Rev. Immunol. *3*, 23–35.

Gosselin, D., Link, V.M., Romanoski, C.E., Fonseca, G.J., Eichenfield, D.Z., Spann, N.J., Stender, J.D., Chun, H.B., Garner, H., Geissmann, F., et al. (2014). Environment drives selection and function of enhancers controlling tissue-specific macrophage identities. Cell *159*, 1327–1340.

Goubau, D., Romieu-Mourez, R., Solis, M., Hernandez, E., Mesplède, T., Lin, R., Leaman, D., and Hiscott, J. (2009). Transcriptional re-programming of primary macrophages reveals distinct apoptotic and anti-tumoral functions of IRF-3 and IRF-7. Eur. J. Immunol. *39*, 527–540.

Grün, D., Lyubimova, A., Kester, L., Wiebrands, K., Basak, O., Sasaki, N., Clevers, H., and van Oudenaarden, A. (2015). Single-cell messenger RNA sequencing reveals rare intestinal cell types. Nature *525*, 251–255.

Guiducci, C., Vicari, A.P., Sangaletti, S., Trinchieri, G., and Colombo, M.P. (2005). Redirecting in vivo elicited tumor infiltrating macrophages and dendritic cells towards tumor rejection. Cancer Res. *65*, 3437–3446.

Hagemann, T., Wilson, J., Burke, F., Kulbe, H., Li, N.F., Plüddemann, A., Charles, K., Gordon, S., and Balkwill, F.R. (2006). Ovarian cancer cells polarize macrophages toward a tumor-associated phenotype. J. Immunol. *176*, 5023–5032.

Hagemann, T., Lawrence, T., McNeish, I., Charles, K.A., Kulbe, H., Thompson, R.G., Robinson, S.C., and Balkwill, F.R. (2008). “Re-educating” tumor-associated macrophages by targeting NF-kappaB. J. Exp. Med. *205*, 1261–1268.

Hansson, G.K., and Hermansson, A. (2011). The immune system in atherosclerosis. Nat. Immunol. *12*, 204–212.

Hashimoto, D., Chow, A., Noizat, C., Teo, P., Beasley, M.B., Leboeuf, M., Becker, C.D., See, P., Price, J., Lucas, D., et al. (2013). Tissue-resident macrophages self-maintain locally throughout adult life with minimal contribution from circulating monocytes. Immunity *38*, 792–804.

Huang, S., Guo, Y.-P., May, G., and Enver, T. (2007). Bifurcation dynamics in lineage-commitment in bipotent progenitor cells. Dev. Biol. *305*, 695–713.

Ikegami, M., Ueda, T., Hull, W., Whitsett, J.A., Mulligan, R.C., Dranoff, G., and Jobe, A.H. (1996). Surfactant metabolism in transgenic mice after granulocyte macrophage-colony stimulating factor ablation. Am. J. Physiol. *270*, L650–L658.

Jaitin, D.A., Kenigsberg, E., Keren-Shaul, H., Elefant, N., Paul, F., Zaretsky, I., Mildner, A., Cohen, N., Jung, S., Tanay, A., et al. (2014). Massively parallel single-cell RNA-seq for marker-free decomposition of tissues into cell types. Science *343*, 776–779.

Ju, C., and Tacke, F. (2016). Hepatic macrophages in homeostasis and liver diseases: from pathogenesis to novel therapeutic strategies. Cell. Mol. Immunol. *13*, 316–327.

Kanda, H., Tateya, S., Tamori, Y., Kotani, K., Hiasa, K.-I., Kitazawa, R., Kitazawa, S., Miyachi, H., Maeda, S., Egashira, K., et al. (2006). MCP-1 contributes to macrophage infiltration into adipose tissue, insulin resistance, and hepatic steatosis in obesity. J. Clin. Invest. *116*, 1494–1505.

Kiernan, J.A. (2000). Formaldehyde, Formalin, Paraformaldehyde And Glutaraldehyde: What They Are And What They Do. Micros. Today *8*, 8–13.

Kim, D., Pertea, G., Trapnell, C., Pimentel, H., Kelley, R., and Salzberg, S.L. (2013). TopHat2: accurate alignment of transcriptomes in the presence of insertions, deletions and gene fusions. Genome Biol. *14*, R36.

Kim, H.Y., DeKruyff, R.H., and Umetsu, D.T. (2010). The many paths to asthma: phenotype shaped by innate and adaptive immunity. Nat. Immunol. *11*, 577–584.

Klein, A.M., Mazutis, L., Akartuna, I., Tallapragada, N., Veres, A., Li, V., Peshkin, L., Weitz, D.A., and Kirschner, M.W. (2015). Droplet barcoding for single-cell transcriptomics applied to embryonic stem cells. Cell *161*, 1187–1201.

Kohyama, M., Ise, W., Edelson, B.T., Wilker, P.R., Hildner, K., Mejia, C., Frazier, W.A., Murphy, T.L., and Murphy, K.M. (2009). Role for Spi-C in the development of red pulp macrophages and splenic iron homeostasis. Nature *457*, 318–321.

Kosteli, A., Sugaru, E., Haemmerle, G., Martin, J.F., Lei, J., Zechner, R., and Ferrante, A.W., Jr (2010). Weight loss and lipolysis promote a dynamic immune response in murine adipose tissue. J. Clin. Invest. *120*, 3466–3479.

Lavin, Y., Winter, D., Blecher-Gonen, R., David, E., Keren-Shaul, H., Merad, M., Jung, S., and Amit, I. (2014). Tissue-resident macrophage enhancer landscapes are shaped by the local microenvironment. Cell *159*, 1312–1326.

Li, H., Handsaker, B., Wysoker, A., Fennell, T., Ruan, J., Homer, N., Marth, G., Abecasis, G., Durbin, R., and 1000 Genome Project Data Processing Subgroup (2009). The Sequence Alignment/Map format and SAMtools. Bioinformatics *25*, 2078–2079.

Libby, P., Ridker, P.M., and Hansson, G.K. (2011). Progress and challenges in translating the biology of atherosclerosis. Nature *473*, 317–325.

Liu, Y.-C., Zou, X.-B., Chai, Y.-F., and Yao, Y.-M. (2014). Macrophage Polarization in Inflammatory Diseases. International Journal of Biological Sciences *10*, 520–529.

Love, M.I., Huber, W., and Anders, S. (2014). Moderated estimation of fold change and dispersion for RNA-seq data with DESeq2. Genome Biol. *15*, 550.

Lu, L., Li, J., Moussaoui, M., and Boix, E. (2018). Immune Modulation by Human Secreted RNases at the Extracellular Space. Front. Immunol. *9*, 1012.

Lumeng, C.N., Bodzin, J.L., and Saltiel, A.R. (2007). Obesity induces a phenotypic switch in adipose tissue macrophage polarization. J. Clin. Invest. *117*, 175–184.

Lumeng, C.N., DelProposto, J.B., Westcott, D.J., and Saltiel, A.R. (2008). Phenotypic switching of adipose tissue macrophages with obesity is generated by spatiotemporal differences in macrophage subtypes. Diabetes *57*, 3239–3246.

Mantovani, A., Sozzani, S., Locati, M., Allavena, P., and Sica, A. (2002). Macrophage polarization: tumor-associated macrophages as a paradigm for polarized M2 mononuclear phagocytes. Trends Immunol. *23*, 549–555.

Mantovani, A., Sica, A., Sozzani, S., Allavena, P., Vecchi, A., and Locati, M. (2004). The chemokine system in diverse forms of macrophage activation and polarization. Trends Immunol. *25*, 677–686.

Mantovani, A., Germano, G., Marchesi, F., Locatelli, M., and Biswas, S.K. (2011). Cancer-promoting tumor-associated macrophages: new vistas and open questions. Eur. J. Immunol. *41*, 2522–2525.

Martinez, F.O., and Gordon, S. (2014). The M1 and M2 paradigm of macrophage activation: time for reassessment. F1000Prime Rep. *6*, 13.

Melgert, B.N., Oriss, T.B., Qi, Z., Dixon-McCarthy, B., Geerlings, M., Hylkema, M.N., and Ray, A. (2010). Macrophages: regulators of sex differences in asthma? Am. J. Respir. Cell Mol. Biol. *42*, 595–603.

Melgert, B.N., ten Hacken, N.H., Rutgers, B., Timens, W., Postma, D.S., and Hylkema, M.N. (2011). More alternative activation of macrophages in lungs of asthmatic patients. J. Allergy Clin. Immunol. *127*, 831–833.

Mestas, J., and Hughes, C.C.W. (2004). Of mice and not men: differences between mouse and human immunology. J. Immunol. *172*, 2731–2738.

Mills, C.D., and Ley, K. (2014). M1 and M2 macrophages: the chicken and the egg of immunity. J. Innate Immun. *6*, 716–726.

Mills, C.D., Kincaid, K., Alt, J.M., Heilman, M.J., and Hill, A.M. (2000). M-1/M-2 macrophages and the Th1/Th2 paradigm. J. Immunol. *164*, 6166–6173.

Mosser, D.M., and Edwards, J.P. (2008). Exploring the full spectrum of macrophage activation. Nat. Rev. Immunol. *8*, 958–969.

Murray, P.J., and Wynn, T.A. (2011). Protective and pathogenic functions of macrophage subsets. Nat. Rev. Immunol. *11*, 723–737.

Murray, P.J., Allen, J.E., Biswas, S.K., Fisher, E.A., Gilroy, D.W., Goerdt, S., Gordon, S., Hamilton, J.A., Ivashkiv, L.B., Lawrence, T., et al. (2014). Macrophage activation and polarization: nomenclature and experimental guidelines. Immunity *41*, 14–20.

Nakamura, A., Ebina-Shibuya, R., Itoh-Nakadai, A., Muto, A., Shima, H., Saigusa, D., Aoki, J., Ebina, M., Nukiwa, T., and Igarashi, K. (2013). Transcription repressor Bach2 is required for pulmonary surfactant homeostasis and alveolar macrophage function. J. Exp. Med. *210*, 2191–2204.

Nathan, C.F., Murray, H.W., Wiebe, M.E., and Rubin, B.Y. (1983). Identification of interferon-gamma as the lymphokine that activates human macrophage oxidative metabolism and antimicrobial activity. J. Exp. Med. *158*, 670–689.

Nayak, D., Roth, T.L., and McGavern, D.B. (2014). Microglia development and function. Annu. Rev. Immunol. *32*, 367–402.

Nguyen, K.D., Qiu, Y., Cui, X., Goh, Y.P.S., Mwangi, J., David, T., Mukundan, L., Brombacher, F., Locksley, R.M., and Chawla, A. (2011). Alternatively activated macrophages produce catecholamines to sustain adaptive thermogenesis. Nature *480*, 104–108.

Okabe, Y., and Medzhitov, R. (2014). Tissue-specific signals control reversible program of localization and functional polarization of macrophages. Cell *157*, 832–844.

Olefsky, J.M., and Glass, C.K. (2010). Macrophages, inflammation, and insulin resistance. Annu. Rev. Physiol. *72*, 219–246.

Paolicelli, R.C., Bolasco, G., Pagani, F., Maggi, L., Scianni, M., Panzanelli, P., Giustetto, M., Ferreira, T.A., Guiducci, E., Dumas, L., et al. (2011). Synaptic pruning by microglia is necessary for normal brain development. Science *333*, 1456–1458.

Pliner, H.A., Shendure, J., and Trapnell, C. (2019). Supervised classification enables rapid annotation of cell atlases. Nat. Methods *16*, 983–986.

Qian, B.-Z., and Pollard, J.W. (2010). Macrophage diversity enhances tumor progression and metastasis. Cell *141*, 39–51.

Qiu, X., Mao, Q., Tang, Y., Wang, L., Chawla, R., Pliner, H.A., and Trapnell, C. (2017). Reversed graph embedding resolves complex single-cell trajectories. Nat. Methods *14*, 979–982.

Quinlan, A.R., and Hall, I.M. (2010). BEDTools: a flexible suite of utilities for comparing genomic features. Bioinformatics *26*, 841–842.

R Core Team (2018). R: A language and environment for statistical computing. R Foundation for Statistical Computing, Vienna, Austria. Available online at https://www.R-project.org/.

Roberts, A., Trapnell, C., Donaghey, J., Rinn, J.L., and Pachter, L. (2011a). Improving RNA-Seq expression estimates by correcting for fragment bias. Genome Biol. *12*, R22.

Roberts, A., Pimentel, H., Trapnell, C., and Pachter, L. (2011b). Identification of novel transcripts in annotated genomes using RNA-Seq. Bioinformatics *27*, 2325–2329.

Rosenberg, A.B., Roco, C.M., Muscat, R.A., Kuchina, A., Sample, P., Yao, Z., Graybuck, L.T., Peeler, D.J., Mukherjee, S., Chen, W., et al. (2018). Single-cell profiling of the developing mouse brain and spinal cord with split-pool barcoding. Science *360*, 176–182.

Schneemann, M., and Schoeden, G. (2007). Macrophage biology and immunology: man is not a mouse. J. Leukoc. Biol. *81*, 579-580.

Schneemann, M., and Schoedon, G. (2002). Species differences in macrophage NO production are important. Nat. Immunol. *3*, 102.

Shalek, A.K., Satija, R., Adiconis, X., Gertner, R.S., Gaublomme, J.T., Raychowdhury, R., Schwartz, S., Yosef, N., Malboeuf, C., Lu, D., et al. (2013). Single-cell transcriptomics reveals bimodality in expression and splicing in immune cells. Nature *498*, 236–240.

Sica, A., and Mantovani, A. (2012). Macrophage plasticity and polarization: in vivo veritas. J. Clin. Invest. *122*, 787–795.

Sica, A., Invernizzi, P., and Mantovani, A. (2014). Macrophage plasticity and polarization in liver homeostasis and pathology. Hepatology *59*, 2034–2042.

Slovinsky, W.S., Romero, F., Sales, D., Shaghaghi, H., and Summer, R. (2019). The involvement of GM-CSF deficiencies in parallel pathways of pulmonary alveolar proteinosis and the alcoholic lung. Alcohol *80*, 73–79.

Smith, T.D., Tse, M.J., Read, E.L., and Liu, W.F. (2016). Regulation of macrophage polarization and plasticity by complex activation signals. Integr. Biol. *8*, 946–955.

Stein, M., Keshav, S., Harris, N., and Gordon, S. (1992). Interleukin 4 potently enhances murine macrophage mannose receptor activity: a marker of alternative immunologic macrophage activation. J. Exp. Med. *176*, 287–292.

Stout, R.D., and Suttles, J. (1997). T cell signaling of macrophage function in inflammatory disease. Front. Biosci. *2*, d197–d206.

Stout, R.D., and Suttles, J. (2004). Functional plasticity of macrophages: reversible adaptation to changing microenvironments. J. Leukoc. Biol. *76*, 509–513.

Stout, R.D., Jiang, C., Matta, B., Tietzel, I., Watkins, S.K., and Suttles, J. (2005). Macrophages sequentially change their functional phenotype in response to changes in microenvironmental influences. J. Immunol. *175*, 342–349.

Subramanian, V., and Ferrante, A.W., Jr (2009). Obesity, inflammation, and macrophages. Nestle Nutr. Workshop Ser. Pediatr. Program. *63*, 151–159; discussion 159–162, 259–268.

Suzuki, T., Arumugam, P., Sakagami, T., Lachmann, N., Chalk, C., Sallese, A., Abe, S., Trapnell, C., Carey, B., Moritz, T., et al. (2014). Pulmonary macrophage transplantation therapy. Nature *514*, 450–454.

Tang, F., Barbacioru, C., Bao, S., Lee, C., Nordman, E., Wang, X., Lao, K., and Surani, M.A. (2010). Tracing the derivation of embryonic stem cells from the inner cell mass by single-cell RNA-Seq analysis. Cell Stem Cell *6*, 468–478.

Thomas, A.C., and Mattila, J.T. (2014). “Of mice and men”: arginine metabolism in macrophages. Front. Immunol. *5*, 479.

Trapnell, C. (2015). Defining cell types and states with single-cell genomics. Genome Res. *25*, 1491–1498.

Trapnell, B.C., and Whitsett, J.A. (2002). GM-CSF regulates pulmonary surfactant homeostasis and alveolar macrophage-mediated innate host defense. Annu. Rev. Physiol. *64*, 775–802.

Trapnell, B.C., Whitsett, J.A., and Nakata, K. (2003). Pulmonary alveolar proteinosis. N. Engl. J. Med. *349*, 2527–2539.

Trapnell, C., Williams, B.A., Pertea, G., Mortazavi, A., Kwan, G., van Baren, M.J., Salzberg, S.L., Wold, B.J., and Pachter, L. (2010). Transcript assembly and quantification by RNA-Seq reveals unannotated transcripts and isoform switching during cell differentiation. Nat. Biotechnol. *28*, 511–515.

Trapnell, C., Hendrickson, D.G., Sauvageau, M., Goff, L., Rinn, J.L., and Pachter, L. (2013). Differential analysis of gene regulation at transcript resolution with RNA-seq. Nat. Biotechnol. *31*, 46–53.

Trapnell, C., Cacchiarelli, D., Grimsby, J., Pokharel, P., Li, S., Morse, M., Lennon, N.J., Livak, K.J., Mikkelsen, T.S., and Rinn, J.L. (2014). The dynamics and regulators of cell fate decisions are revealed by pseudotemporal ordering of single cells. Nat. Biotechnol. *32*, 381–386.

Treutlein, B., Brownfield, D.G., Wu, A.R., Neff, N.F., Mantalas, G.L., Espinoza, F.H., Desai, T.J., Krasnow, M.A., and Quake, S.R. (2014). Reconstructing lineage hierarchies of the distal lung epithelium using single-cell RNA-seq. Nature *509*, 371–375.

Watkins, S.K., Li, B., Richardson, K.S., Head, K., Egilmez, N.K., Zeng, Q., Suttles, J., and Stout, R.D. (2009). Rapid release of cytoplasmic IL-15 from tumor-associated macrophages is an initial and critical event in IL-12-initiated tumor regression. Eur. J. Immunol. *39*, 2126–2135.

Weisberg, S.P., McCann, D., Desai, M., Rosenbaum, M., Leibel, R.L., and Ferrante, A.W., Jr (2003). Obesity is associated with macrophage accumulation in adipose tissue. J. Clin. Invest. *112*, 1796–1808.

Wickham, H. (2009). ggplot2: Elegant Graphics for Data Analysis (New York: Springer).

Wills, Q.F., Livak, K.J., Tipping, A.J., Enver, T., Goldson, A.J., Sexton, D.W., and Holmes, C. (2013). Single-cell gene expression analysis reveals genetic associations masked in whole-tissue experiments. Nat. Biotechnol. *31*, 748–752.

Wong, S.-C., Puaux, A.-L., Chittezhath, M., Shalova, I., Kajiji, T.S., Wang, X., Abastado, J.-P., Lam, K.-P., and Biswas, S.K. (2010). Macrophage polarization to a unique phenotype driven by B cells. Eur. J. Immunol. *40*, 2296–2307.

Wynn, T.A., Chawla, A., and Pollard, J.W. (2013). Macrophage biology in development, homeostasis and disease. Nature *496*, 445–455.

Xu, H., Barnes, G.T., Yang, Q., Tan, G., Yang, D., Chou, C.J., Sole, J., Nichols, A., Ross, J.S., Tartaglia, L.A., et al. (2003). Chronic inflammation in fat plays a crucial role in the development of obesity-related insulin resistance. J. Clin. Invest. *112*, 1821–1830.

Xue, J., Schmidt, S.V., Sander, J., Draffehn, A., Krebs, W., Quester, I., De Nardo, D., Gohel, T.D., Emde, M., Schmidleithner, L., et al. (2014). Transcriptome-based network analysis reveals a spectrum model of human macrophage activation. Immunity *40*, 274–288.

Yeramian, A., Martin, L., Serrat, N., Arpa, L., Soler, C., Bertran, J., McLeod, C., Palacín, M., Modolell, M., Lloberas, J., et al. (2006). Arginine transport via cationic amino acid transporter 2 plays a critical regulatory role in classical or alternative activation of macrophages. J. Immunol. *176*, 5918–5924.

Yona, S., Kim, K.-W., Wolf, Y., Mildner, A., Varol, D., Breker, M., Strauss-Ayali, D., Viukov, S., Guilliams, M., Misharin, A., et al. (2013). Fate mapping reveals origins and dynamics of monocytes and tissue macrophages under homeostasis. Immunity *38*, 79–91.

Yoshida, M., Ikegami, M., Reed, J.A., Chroneos, Z.C., and Whitsett, J.A. (2001). GM-CSF regulates protein and lipid catabolism by alveolar macrophages. Am. J. Physiol. Lung Cell. Mol. Physiol. *280*, L379–L386.

Zhang, Y., Liu, T., Meyer, C.A., Eeckhoute, J., Johnson, D.S., Bernstein, B.E., Nusbaum, C., Myers, R.M., Brown, M., Li, W., et al. (2008). Model-based analysis of ChIP-Seq (MACS). Genome Biol. *9*, R137.

Zimmermann, H.W., Trautwein, C., and Tacke, F. (2012). Functional role of monocytes and macrophages for the inflammatory response in acute liver injury. Front. Physiol. *3*, 56.

VITA

Serena Liu grew up in Bellevue, Washington. She received her B.A. in Biology and Economics *summa cum laude* from Dartmouth College in 2014, and graduated as co-valedictorian of her class. While at Dartmouth, she worked in the lab of Thomas Jack and studied the genetics of flower development in *Arabidopsis thaliana*. She started her Ph.D. work in Genome Sciences at the University of Washington in 2014. Her graduate work with Cole Trapnell focuses on characterizing the processes of macrophage polarization and repolarization using single-cell transcriptomics. When not in lab, Serena spends her time pursuing varied arts and crafts projects and practicing ballroom and swing dancing.